CANCER

Small-molecule inhibition of YTHDC1 as a strategy against acute myeloid leukemia in mouse models

Hailin Zhang[1,2]†, Yueshan Li[1,2]†, Yin Zhao[3]†, Falu Wang[1,2,4]†, Guifeng Lin[1,2]†, Ting Niu[5]†, He Li[5]†, Yueyue Li[1,2]†, Lina Liu[3]†, Yue Liang[3], Yu Shen[3], Yuyao Yi[5], Hui Zhou[5], Shang Lou[3], Yishan Ye[3], Yanmin He[6], Ruicheng Yang[1,2], Rui Yao[1,2], Chenyu Tian[1,2], Pei Zhou[7], Mengdan Wu[1], Mingxin Chen[1], Haixing Xu[1,2], Jing You[1,2], Yi Liao[5], Chenlu Yang[5], Ailin Zhao[5], Chong Chen[1], Linli Li[7]*, Shanshan Pei[3]*, Shengyong Yang[1,2]*

Dysregulation of RNA N^6-methyladenosine (m^{6}A) readers has been linked to various diseases, but the therapeutic potential of small-molecule inhibitors targeting them is of interest. Here, we reported the identification and characterization of a potent and selective first-in-class inhibitor (YL-5092) of YTHDC1, a nuclear RNA m^{6}A reader. We provided a high-resolution cocrystal structure of the YTHDC1–YL-5092 complex. In acute myeloid leukemia (AML) models, YL-5092 blocked the binding of YTHDC1 to its m^{6}A substrates and reduced mRNA stability, resulting in apoptosis of AML cells and myeloid differentiation. In multiple xenograft models of AML representing disease heterogeneity, YL-5092 alone or in combination with standard AML therapy eliminated leukemia and extended survival. Moreover, YL-5092 functionally impaired leukemia stem cells yet spared normal hematopoietic counterparts. Collectively, our work demonstrates the efficacy of a selective YTHDC1 inhibitor and suggests that targeting of m^{6}A readers is a potential strategy in the treatment of hematologic cancers.

INTRODUCTION

N^6-methyladenosine (m^{6}A) is the most abundant posttranscriptional modification in eukaryotic mRNA, which plays essential roles in regulating mRNA metabolism and function (*1*, *2*). The m^{6}A modification is dynamic and reversible: m^{6}A is installed on mRNA by methyltransferases ("writers") and removed by demethylases ("erasers") (*2*–*4*). The fate and functions of m^{6}A-modified mRNAs (m^{6}A-mRNAs) heavily rely on various m^{6}A-binding proteins ("readers"), which recognize and generate functional signals from m^{6}A-mRNAs (*2*, *5*, *6*). Currently, five YT521-B homology (YTH) domain–containing proteins (YTHDC1 and YTHDC2 and YTHDF1 to YTHDF3) and several additional proteins, including insulin-like growth factor 2 mRNA binding proteins (IGF2BP1 to IGF2BP3) and heterogeneous nuclear ribonucleoproteins A2/B1 (HNRNPA2B1), have been identified as readers of m^{6}A-mRNAs (*7*–*9*). These m^{6}A readers have been demonstrated to play important roles in a wide range of physiological and pathological processes, particularly in regulating hematopoietic stem cell (HSC) function and in the pathogenesis of acute myeloid leukemia (AML) (*10*–*18*).

YTHDC1, as an important reader of m^{6}A-mRNAs, has distinct roles in regulating nuclear RNA splicing, alternative polyadenylation, nuclear export, and decay (*12*, *19*–*25*). Dysregulation of YTHDC1 is associated with a number of pathologies, particularly AML (*12*, *26*–*28*). YTHDC1 is overexpressed in AML cells and is essential for AML cell proliferation and survival (*12*, *13*). Further studies have shown that the genetic deletion of YTHDC1 markedly suppresses AML development and maintenance as well as self-renewal of leukemia stem cells (LSCs) in mice (*12*). YTHDC1 has thus been considered as a potential target for the treatment of AML, and small-molecule inhibitors of YTHDC1 may be promising agents against AML. Nevertheless, to our knowledge, no potent YTHDC1 inhibitors demonstrating in vivo efficacy have been reported to date (*29*–*31*). The work here presents the discovery and characterization of a first-in-class small-molecule inhibitor of YTHDC1 and demonstrates its potential in the treatment of AML.

RESULTS

Discovery and characterization of YTHDC1 inhibitor YL-5092

To identify YTHDC1 inhibitors, we established a fluorescence polarization (FP)–based screening system and screened our in-house chemical library containing about 25,000 compounds. Only one compound, Hit-1 [an extracellular signal–regulated kinase 5 (ERK5) inhibitor] (*32*), showed inhibitory activity against YTHDC1 with a half-maximum inhibitory concentration (IC_{50}) of 5.50 μM (Fig. 1A and fig. S1A). The activity of Hit-1 was validated by a differential scanning fluorimetry (DSF) assay, which gave a thermal shift (ΔT_m) of 2.8°C at a concentration of 100 μM (fig. S1B), indicating direct binding between Hit-1 and YTHDC1. Next, we solved the cocrystal structure of the YTH domain of YTHDC1 in complex with Hit-1 by x-ray crystallography at a resolution of 2.4 Å [Protein Data Bank (PDB) entry 9V84; table S1]. The results show that the 2-bromo-6-fluorobenzene group of Hit-1 occupies the aromatic cage formed by W377, W428, L430, and L439 (fig. S1, C and D), which is also the m^{6}A binding site (*33*). The remaining part of Hit-1 extends into a groove connected with the aromatic cage, formed by one α helix (α3 helix) and three β sheets. Further testing showed that Hit-1 exhibited no detectable activity against other YTH family members (YTHDC2 and YTHDF1 to YTHDF3) (fig. S1E). Molecular docking analyses were performed

[1]Department of Biotherapy, Cancer Center and State Key Laboratory of Biotherapy, West China Hospital, Sichuan University, Chengdu, Sichuan 610041, China. [2]New Cornerstone Science Laboratory, West China Hospital, Sichuan University, Chengdu, Sichuan 610041, China. [3]Bone Marrow Transplantation Center of the First Affiliated Hospital & Liangzhu Laboratory, Zhejiang University School of Medicine, Hangzhou, Zhejiang 311121, China. [4]School of Pharmacy, Xiamen Medical College, Xiamen, Fujian 361023, China. [5]Department of Hematology, West China Hospital, Sichuan University, Chengdu, Sichuan 610041, China. [6]Institute of Transfusion Medicine, Blood Center of Zhejiang Province, Hangzhou, Zhejiang 310052, China. [7]Key Laboratory of Drug-Targeting and Drug Delivery System of the Education Ministry, West China School of Pharmacy, Sichuan University, Chengdu 610041, China.
†These authors contributed equally to this work.
*Corresponding author. Email: yangsy@scu.edu.cn (S.Y.); shanshan.pei@zju.edu.cn (S.P.); lilinli@scu.edu.cn (L. Li)

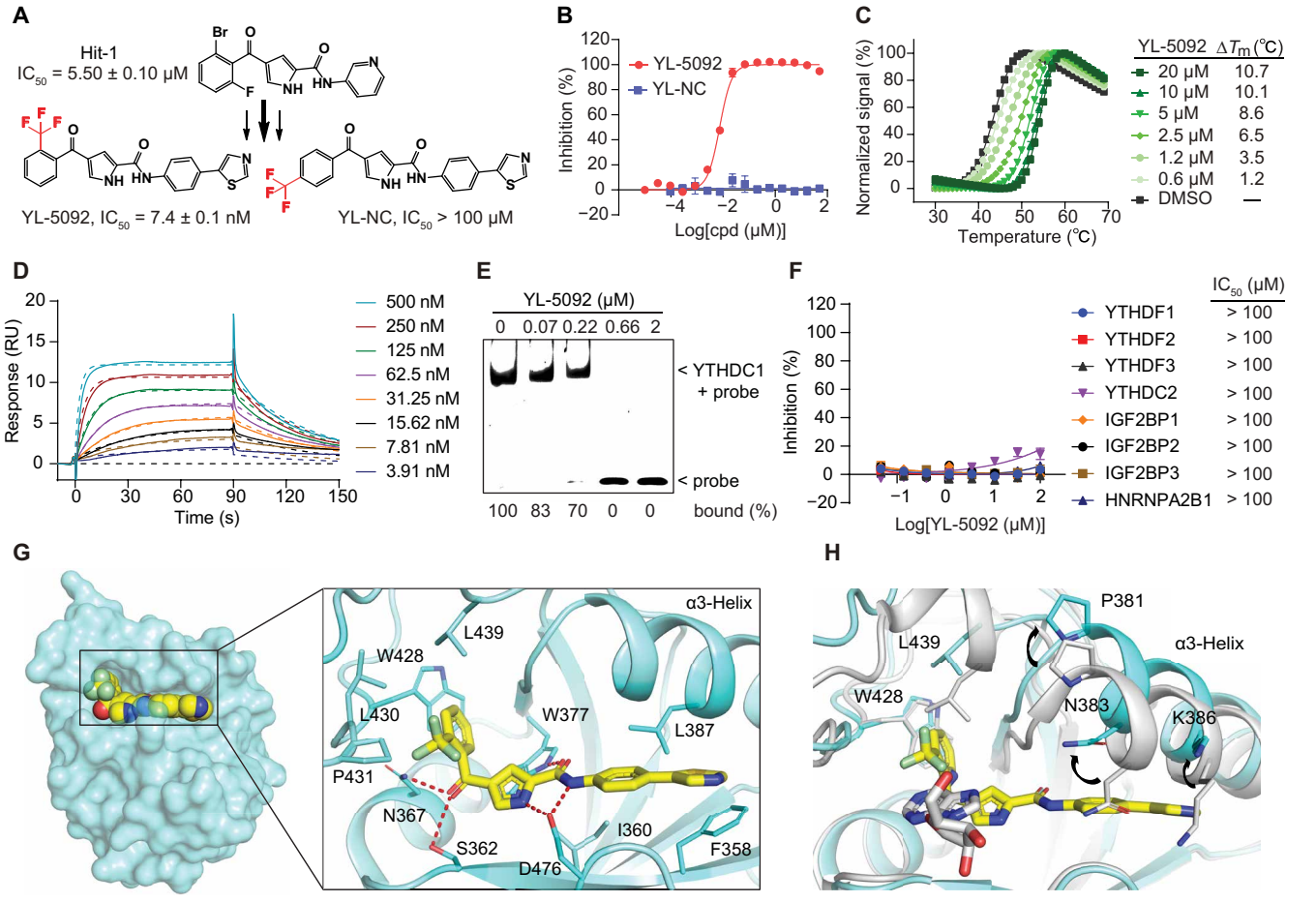

Fig. 1. Bioactivity and structural characterization of the YTHDC1 inhibitor YL-5092. (**A**) Chemical structures and bioactivities against YTHDC1, of the initial hit (Hit-1), the optimized compound (YL-5092), and its inactive isomer (YL-NC). (**B**) Dose-activity curves of compounds YL-5092 and YL-NC measured by the FP assay ($n = 3$). The IC_{50} values were determined using a four-parameter logistic equation in GraphPad Prism 8.0. (**C**) Stabilizing effect of YL-5092 on the YTHDC1 YTH domain protein measured by the DSF assay ($n = 3$). The T_m values were assessed using a Boltzmann equation in GraphPad Prism 8.0. (**D**) SPR binding data for the interaction of YL-5092 with immobilized YTHDC1. (**E**) EMSAs for YTHDC1 in the presence of increasing concentrations of YL-5092 (0.07 to 2.00 μM). (**F**) Bioactivities of YL-5092 against RNA m^6A reader proteins, detected by the FP assay. (**G**) Binding mode of YTHDC1–YL-5092 determined by the crystal structure (PDB ID: 9MB3). Red dashed lines indicate hydrogen bonds (some residues are omitted for viewing clarity). (**H**) Superposition of the YTHDC1–YL-5092 complex (YTHDC1 in bright blue and YL-5092 in yellow) with m^6A bound structure (gray) (PDB ID: 6ZCN). All data were obtained from three independent experiments. Data are shown as averages ± SD.

to investigate Hit-1's binding preference for YTHDC1. These analyses revealed markedly higher scoring function values—a proxy for predicted binding affinity—for Hit-1 with YTHDC1 compared with other YTH proteins (table S2), supporting its selective binding mechanism.

To improve the potency of Hit-1, a structure-guided stepwise optimization process was carried out. According to the x-ray crystal structure, the middle part of Hit-1 (namely, 4-acetyl-1*H*-pyrrole-2-carboxamide) forms important hydrogen bonding interactions with YTHDC1. We thus maintained the middle part and optimized the two terminal groups: 2-bromo-6-fluorophenyl (R_1) and pyridine (R_2). In the first step, we fixed R_2 as pyridine and varied R_1 (fig. S2). Adding a fluorine substitution at site 4 or 5 of phenyl (R_1) caused a complete loss of activity (C-2 and C-3; fig. S2), indicating substitutions at these sites being unfavorable because of limited space in the aromatic cage (fig. S1D). As expected, after removing 6-F of R_1, the activity of the leading compound C-4 increased noticeably. However, upon further removal of 2-Br, the activity of the resulting compound (C-5) decreased substantially, indicating the importance of 2-Br substitution. This is understandable because it locates outside of the aromatic cage and forms hydrophobic interactions with resides L380, P431, and M434 (fig. S1D). Next, different bulky groups were used to replace 2-Br, which generated six new compounds (C-6 to C-11). Compound C-8 with a medium-size group (2-CF_3) showed a higher potency than others with smaller or bulkier substituents because the medium-sized 2-CF_3 can form good interactions but avoid steric repulsion with surrounding residues. In the second step, we fixed R_1 as the optimal 2-trifluoromethyl phenyl group and optimized R_2. The replacement of the original R_2 group (pyridine) with a phenyl group (C-12) increased the potency. We then added a fluoride substitution at ortho-, meta-, or para-position and synthesized three compounds (C-13, C-14, and C-15). Only compound C-15 with para-fluorine showed an increase in activity, indicating that para-substitution may help improve the bioactivity. Hence, different substituents were used on the para-position, and 23 compounds were prepared. Of them, compound C-29 (YL-5092) with a 4-thiazole moiety displayed the

highest activity with a single-digit nanomolar potency (IC_{50} = 7.4 nM; Fig. 1, A and B).

To verify the bioactivity of YL-5092, several biophysical approaches were used. In the DSF assay, YL-5092 dose dependently stabilized the YTHDC1 protein and displayed a ΔT_m value of 10.7°C at a concentration of 20 μM (Fig. 1C). In the surface plasmon resonance (SPR) assay, it exhibited a high binding affinity with a dissociation constant value of 29.6 nM (Fig. 1D). By electrophoretic mobility shift assay (EMSA), YL-5092 dose-dependently blocked the binding of substrate mimic, indicating a competitive inhibitor of substrate (Fig. 1E).

To facilitate subsequent mechanistic studies, we synthesized an isomer (YL-NC) of YL-5092 with trifluoromethyl in R_1 shifting from ortho- to para-position (namely, 2-CF_3 to 4-CF_3). YL-NC showed no activity against YTHDC1 in any of the assays (Fig. 1, A and B). These indicate that YL-NC is a good negative control, which could be used in the subsequent studies.

Target selectivity of YL-5092

To examine the target selectivity of YL-5092, we adopted the FP assay to test the activity of YL-5092 against other RNA m^6A readers, including YTHDC2, YTHDF1 to YTHDF3, IGF2BP1 to IGF2BP3, and HNRNPA2B1. The results indicated that YL-5092 did not show noticeable activity against any of these readers (IC_{50} > 100 μM; Fig. 1F). Similarly, in the EMSA assay, YL-5092 did not interfere with the binding of other YTH proteins to substrate mimic (fig. S3, A to D). In addition, in the DSF assay, YL-5092 had no discernible effect on the thermal stability of other YTH proteins (fig. S3, E to H) or various bromodomain-containing proteins functioning as readers of acetylated histones (fig. S3I). Furthermore, in a kinase profiling assay, YL-5092 showed no inhibitory effect on a panel of 416 human protein kinases (fig. S3J), including specific confirmation of ERK5 nonresponsiveness [kinase inhibition: IC_{50} > 100 μM (fig. S3K); binding affinity (SPR): no binding (fig. S3L)]. Thus, all data demonstrate that YL-5092 is a highly selective inhibitor of YTHDC1.

Structural understanding of the potency and selectivity of YL-5092

To understand the high potency of YL-5092 against YTHDC1, we solved the cocrystal structure of the YTH domain of YTHDC1 in complex with YL-5092 by x-ray crystallography at a resolution of 1.65 Å (PDB entry 9MB3; table S1). YL-5092 adopts the same binding pose as Hit-1. As expected in the structural optimization process, the 2-trifluoromethyl-phenyl group occupies the aromatic cage consisting of residues W377, W428, L430, and L439, with 2-trifluoromethyl pointing to the outside of the aromatic cage (Fig. 1G). The pyrrole nitrogen and amide nitrogen individually form a hydrogen bond with residues D476. The amide oxygen forms a hydrogen bond with residue W377. Meanwhile, the carbonyl oxygen forms two hydrogen bonds with residues S362 and N367. The 5-phenylthiazole tail forms good hydrophobic interactions with residues I360, L387, and F358. We also noticed a π-π stacking interaction between thiazole and the benzene ring of F358. To validate these structural observations, we introduced mutations in the interacting residues (W428A, D476A, N367A, I360A, S362A, W377F, L430A, and L439A), followed by DSF analysis. The results showed a substantial reduction in binding activity of YL-5092 compared with the wild-type protein (ΔT_m = 10.7°C): W377F (ΔT_m = 5.9°C), W428A (ΔT_m = 0.7°C), L430A (ΔT_m = 3.9°C), D476A (ΔT_m = 1.3°C), S362A (ΔT_m = 9.3°C), N367A (ΔT_m = 3.5°C), I360A (ΔT_m = 0.5°C), and L439A (ΔT_m = 6.8°C) (fig. S4, A and B). These findings support the proposed cocrystal structure, given that the single mutants exhibited reduced binding activity with YL-5092. Compared with the structures of YTHDC1 bound to an m^6A mimic (PDB: 6ZCN; Fig. 1H) or m^6A-RNA (PDB: 4R3I), the main chain of α3 helix shows an evident outward shift, which enlarges the space between the α3 helix and the three β sheets to accommodate YL-5092 (Fig. 1H). Changing 2-CF_3 to 4-CF_3 in the phenyl group of R_1 likely results in a steric collision with residue W428, leading to the isomer YL-NC to be inactive.

To elucidate the selectivity of YL-5092 for YTHDC1 over other YTH domain family members, we conducted molecular docking analyses of YL-5092 against all YTH family proteins (YTHDC1 and YTHDC2 and YTHDF1 to YTHDF3). The results revealed markedly higher scoring function values for YL-5092 with YTHDC1 compared with the other YTH proteins (table S2), demonstrating its selective binding preference for YTHDC1. Subsequent alignment of the amino acid sequences and three-dimensional (3D) structures of YTH family proteins highlighted key differences. The YTH domain of YTHDC1 shares homology similarities of 50.38, 33.33, 31.82, and 30.3% with that of YTHDC2, YTHDF1, YTHDF2, and YTHDF3, respectively (fig. S5A). Although all YTH proteins adopt a conserved 3D fold, YTHDC2 lacks a critical binding loop within the m^6A recognition pocket (fig. S5B). This structural absence likely prevents YTHDC2 from forming hydrophobic interactions with the 2-trifluoromethyl-phenyl group of YL-5092, explaining the compound's inactivity against YTHDC2. Further structural comparisons between YTHDC1 and YTHDF1 to YTHDF3 revealed distinct residue variations in key regions. Specifically, YTHDF1 to YTHDF3 have a bulkier tryptophan residue (W470, W491, or W497) in place of YTHDC1's L439 within the aromatic cage and a larger arginine residue (R420, R441, or R447) instead of YTHDC1's K386 in the adjacent groove (fig. S5C). These substitutions likely introduce steric clashes that hinder YL-5092 from binding to YTHDF1 to YTHDF3, thereby accounting for the compound's lack of activity against these paralogs.

Target engagement of YL-5092 in living cells

Previous studies have shown that YTHDC1 is an important target in myeloid leukemia (*12*, *13*). Thus, we next wanted to verify whether YL-5092 selectively interacts with YTHDC1 in intact cancer cells using myeloid leukemia as a model. To this end, we performed a cellular thermal shift assay (CETSA), a biophysical technique allowing the direct study of drug (ligand) binding to proteins (targets) in living cells (*34*). Our results showed that YL-5092 treatment could dose-dependently stabilize YTHDC1 without affecting YTHDC2 and YTHDF1 to YTHDF3 in myeloid leukemia cell line MOLM-13 and U937 cells (Fig. 2A and fig. S6, A and B), indicating a selective binding of YL-5092 to YTHDC1 in leukemic cells. In addition, we performed fluorescence recovery after photobleaching (FRAP) assays to assess the mobility of enhanced green fluorescent protein (EGFP)–tagged YTHDC1 in live human embryonic kidney (HEK) 293T cells. YL-5092 treatment markedly enhanced the fluorescence recovery with a normalized half-life recovery time ($t_{1/2}$) shortened from 1.976 to 1.365 s, suggesting that the binding of YTHDC1 with its m^6A-mRNA substrates was hampered by YL-5092 (Fig. 2B). These results demonstrated the specific target engagement of YL-5092 on YTHDC1 in living cells.

We then wanted to assess the biological effects of YL-5092 on known activities of YTHDC1 in leukemia cells. A recent study found YTHDC1 to undergo a liquid-liquid phase separation (LLPS) by

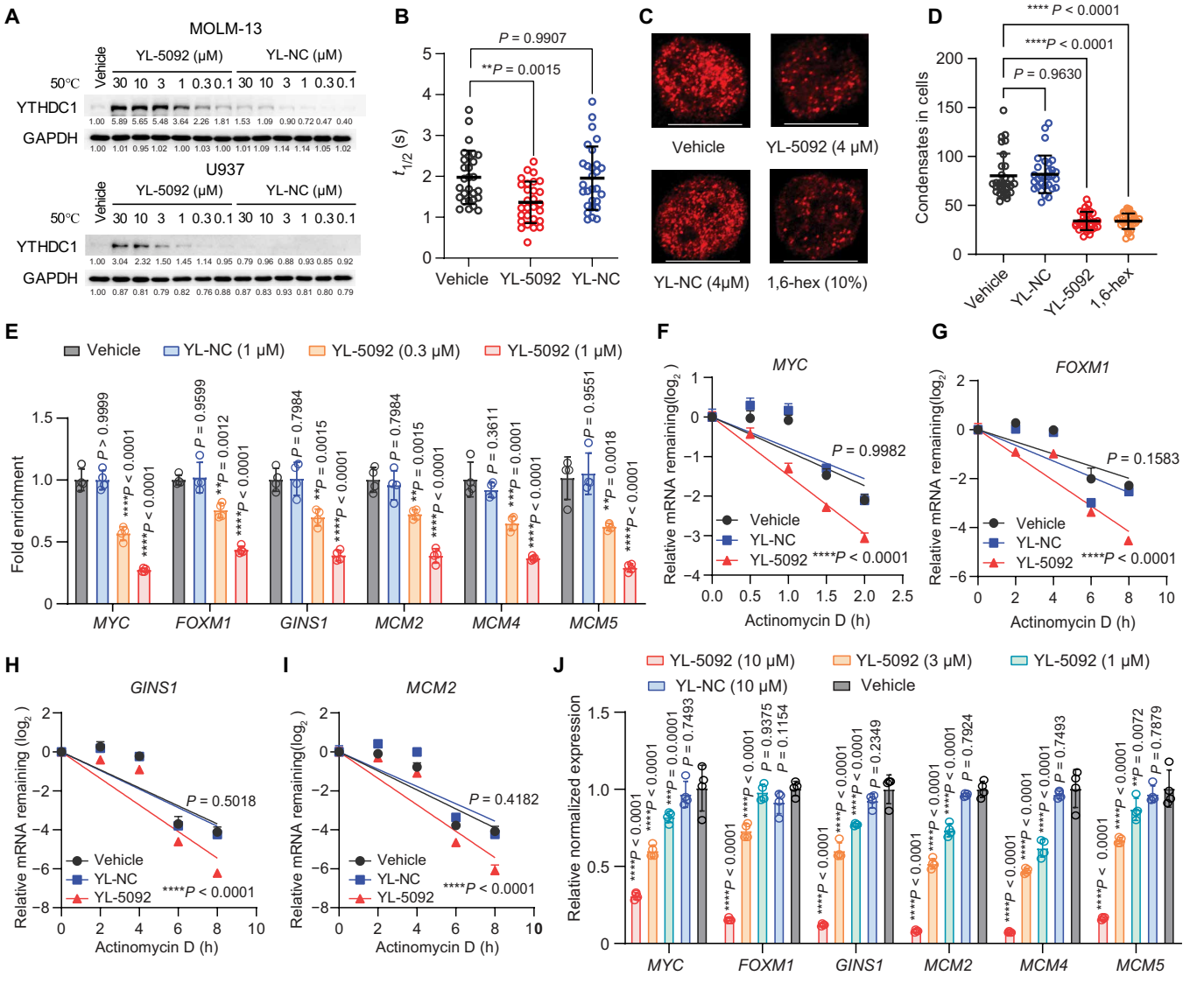

Fig. 2. Target engagement of YTHDC1 inhibitor. (**A**) CETSA assay was carried out with AML cells (MOLM-13 and U937) grown in the presence or absence of YL-5092 or YL-NC for 6 hours ($n = 3$, independent experiments). The labels below the blots represent the normalized intensity. (**B**) FRAP experiment was performed using HEK293T cells expressing EGFP-tagged YTHDC1 ($n = 3$, independent experiments). (**C** and **D**) After different treatments, nuclear condensates in MV4-11 cells were observed by immunofluorescence staining with anti-YTHDC1 antibody. Representative images are shown (C), and condensates in the nucleus were quantified (D) ($n = 3$, independent experiments). Scale bars, 10 μm. (**E**) YTHDC1–RIP-qPCR analysis of YTHDC1 enrichments at mRNAs of the selected target genes in MOLM-13 cells treated with vehicle, YL-5092, or YL-NC ($n = 3$, independent experiments). (**F** to **I**) Effect of YL-5092 treatment on the stability of *MYC* (F), *FOXM1* (G), *GINS1* (H), and *MCM2* (I) mRNAs in MOLM-13 cells by RNA degradation assay ($n = 3$, independent replicates). (**J**) Effect of YL-5092 treatment on the expression of *MYC*, *FOXM1*, *GINS1*, *MCM2*, *MCM4*, and *MCM5* mRNAs in MOLM-13 cells by qRT-PCR ($n = 3$, independent experiments). All data are shown as averages ± SD. The *P* values were analyzed using one-way ANOVA [(B) and (D) and (F) to (I)] and two-way ANOVA [(E) and (J)] compared with the vehicle control group; $^{**}P < 0.01$, $^{***}P < 0.001$, and $^{****}P < 0.0001$. GAPDH, glyceraldehyde-3-phosphate dehydrogenase.

binding to m^{6}A to form dynamic nuclear condensates (*13*, *35*). Thus, we first examined whether YL-5092 can interfere with this event. It appeared that YL-5092 performed equally well as 1,6-hexanediol, a commonly used inhibitor of LLPS (*36*), in substantially inhibiting the LLPS phenotype mediated by YTHDC1 and reducing the formation of nuclear condensates in leukemia cell line MV4-11 cells (Fig. 2, C and D). The negative control YL-NC, however, did not show any effect (Fig. 2, A to D). We then focused our study on the impact of YL-5092 on six well-known substrates of YTHDC1—including *MYC*, *FOXM1*, *GINS1*, *MCM2*, *MCM4*, and *MCM5*—in myeloid leukemia (*12*, *13*). We first examined the impact by RNA immunoprecipitation-quantitative polymerase chain reaction (RIP-qPCR). The results showed that YL-5092 markedly reduced the binding between YTHDC1 and these key substrates required for its leukemogenic function (Fig. 2E). Consequently, the YL-5092–induced loss in binding resulted in substantially decreased stability of *MYC*, *FOXM1*, *GINS1*, *MCM2*, *MCM4*, and *MCM5* transcripts in MOLM-13 cells as revealed by an RNA stability assay (Fig. 2, F to I, and fig. S6, C and D). Subsequently, we observed that

YL-5092 treatment dose-dependently reduced the mRNA levels of all of these genes in the MOLM-13 cells (Fig. 2J). Conversely, in AML cells with *YTHDC1* knockdown, YL-5092 failed to substantially reduce the mRNA stability and relative expression of these target genes (figs. S6, E to L). Together, these data suggest that YL-5092 blocks the binding of YTHDC1 to its key m^{6}A substrates, induces their mRNA instability, and subsequently leads to their transcript loss.

Global effects of YL-5092 on targets of YTHDC1 in AML cells

To comprehensively characterize the global impact of YL-5092–induced YTHDC1 m^{6}A substrate loss in leukemic cells, we next performed RNA sequencing (RNA-seq), analysis of MOLM-13 cells treated with vehicle, YL-5092, or YL-NC. We found that YL-5092 treatment substantially altered the expression of 3761 genes (2045 up and 1716 down), whereas YL-NC treatment minimally affected the transcriptome (Fig. 3A). The differentially expressed genes induced by YL-5092 and mediated by *YTHDC1* knockdown (KD) (*13*) had a marked overlap (52.0% of the *YTHDC1* KD) (Fig. 3B). The nonoverlapped transcriptional changes could reflect kinetic differences between genetic and pharmacological perturbations. Nonetheless, by global gene set enrichment analysis, we identified a collection of gene sets affected by YL-5092 (Fig. 3C). YL-5092 treatment markedly down-regulated MYC targets, E2F targets, and G_2-M checkpoint-related gene sets (Fig. 3C and fig. S7A), which are known to be important for leukemogenesis and tumorigenesis in general (*37*).

Next, to identify potential direct YTHDC1 targets among the dysregulated transcripts, we mapped transcriptome-wide m^{6}A modifications (m^{6}A-seq) in MOLM-13 cells treated with YL-5092 or vehicle. Analysis revealed that global m^{6}A peak distribution and GGACU motif enrichment remained largely unchanged between treatment groups (fig. S7, B to D), demonstrating that YL-5092 does not affect m^{6}A deposition itself. Critically, the integration of the m^{6}A-seq and RNA-seq data revealed specific down-regulation of m^{6}A-modified, but not non–m^{6}A-modified, transcripts upon YL-5092 treatment (fig. S7E), suggesting an on-target effect of YL-5092.

Moreover, to directly evaluate changes in transcript stability, we performed thiol(SH)-linked alkylation for the metabolic sequencing of RNA (SLAM-seq) to measure the degradation of RNA transcripts. Globally, transcript half-lives were substantially reduced in the YL-5092–treated group compared with vehicle (Fig. 3D). In both conditions, m^{6}A-modified transcripts had shorter half-lives than non–m^{6}A-modified ones (vehicle: 2.38 hours versus 2.82 hours; YL-5092: 1.70 hours versus 2.28 hours) (Fig. 3E and fig. S7F). It is worth noting that the reduction in half-life was more substantial for m^{6}A-modified transcripts upon YTHDC1 inhibition, consistent with the hypothesis that YTHDC1 plays a critical role in transcript stabilization. To define the core set of transcripts directly regulated by YTHDC1 via m^{6}A-dependent stability, we performed integrated analyses on four datasets: (i) down-regulated genes from RNA-seq, (ii) transcripts displaying decreased stability induced by 5092 from SLAM-seq, (iii) m^{6}A-modified genes from m^{6}A-seq, and (iv) a published YTHDC1 photoactivatable ribonucleoside–enhanced crosslinking and immunoprecipitation (PAR-CLIP) dataset (*33*). These four-way integration analyses identified 403 overlapping genes representing m^{6}A-modified transcript targets of YTHDC1 that experienced down-regulated expression likely because of altered transcript stability upon treatment with YTHDC1 inhibitor YL-5092 (Fig. 3F). We noticed that previously reported target genes of YTHDC1 such as *MYC*, *GINS1*, *MCM4*, and *FOXM1* were among the overlapping targets (Fig. 3G), which further confirmed YL-5092's on-target specificity. Moreover, the pathway analysis of these 403 core targets revealed substantial enrichment in DNA replication, mismatch repair, and cell cycle pathways (fig. S7G), directly linking YL-5092's antileukemic mechanism to the destabilization of proliferation-related transcripts.

In addition, given that a previous study reported that YTHDC1 regulates mRNA splicing (*23*), we also assessed the impact of YTHDC1 inhibition by YL-5092 on global splicing in AML cells. We identified 3781 different types of alternative splicing events representing 2468 genes in MOLM-13 cells upon YL-5092 treatment [false discovery rate (FDR) < 0.05] (Fig. 3H). Through overlapping analysis of YL-5092–dysregulated genes, m^{6}A-modified transcripts, and YTHDC1-binding targets, we further revealed that 270 m^{6}A-modified transcripts directly bound by YTHDC1 experienced changes in alternative splicing upon exposure to YL-5092 (Fig. 3I). The pathway enrichment analysis of the 270 genes identified RNA splicing, mRNA metabolic regulation, and chromosome segregation among the list (fig. S7H).

Last, we performed ribosome profiling (Ribo-seq) to assess the potential impact of YL-5092 on global translational efficiency. We observed no notable differences in translational efficiency between vehicle and YL-5092 groups (fig. S7I). Subsequent detailed analysis focusing on m^{6}A-modified and m^{6}A-unmodified transcripts also revealed no notable differences in translational efficiency between vehicle- and YL-5092-treated cells (fig. S7, J and K). These results suggest that YTHDC1 inhibition does not markedly alter the translation efficiency of mRNA in leukemic cells. Thus, overall, the impacts of YL-5092 on m^{6}A-modified transcripts are at least composed of three components, including the core set of 403 genes representing a direct destabilizing effect of YL-5092, the 270 genes affected by YL-5092–induced disruption of the RNA splicing function of YTHDC1, and the majority of nonoverlapped transcriptome changes likely downstream of YL-5092–induced suppression of primary targets such as transcription factors *MYC*, *FOXM1*, and *GINS1*.

In vitro antileukemic activity of YL-5092

Given the strong YTHDC1 inhibitory effects in leukemic cells, we next examined the in vitro anti-leukemia activity of YL-5092 in a collection of AML cell lines and primary AML specimens representing complex disease heterogeneity of human AML, including seven leukemic cell lines (MV4-11, HL-60, MOLM-13, THP-1, KG-1, U937, and OCI-AML3) and five primary human AML specimens of various AML genotypes and phenotypes (table S3). Through initial viability assay, all the tested AML cell lines and primary samples were very sensitive to YL-5092, with IC_{50} values in the range of 0.28 to 2.87 μM (Fig. 4, A and B), but entirely resistant to YL-NC (IC_{50} > 50 μM) (table S4).

To better dissect the antileukemic activity of YL-5092 in AML cells, flow cytometry was conducted to examine the specific effects of YL-5092 on cell cycle, apoptosis, and myeloid differentiation. The results showed that treatment with YL-5092, but not YL-NC, substantially induced MOLM-13 cell cycle arrest at G_0-G_1 phase (Fig. 4C), apoptosis (Fig. 4D and fig. S8), and myeloid differentiation (Fig. 4E) in a dose-dependent manner. In addition, to assess the impact of YL-5092 on different AML subtypes, we evaluated the sensitivity of 16 primary AML specimens from our laboratory to YL-5092. For comparative analysis, drug sensitivity was quantified using the area under

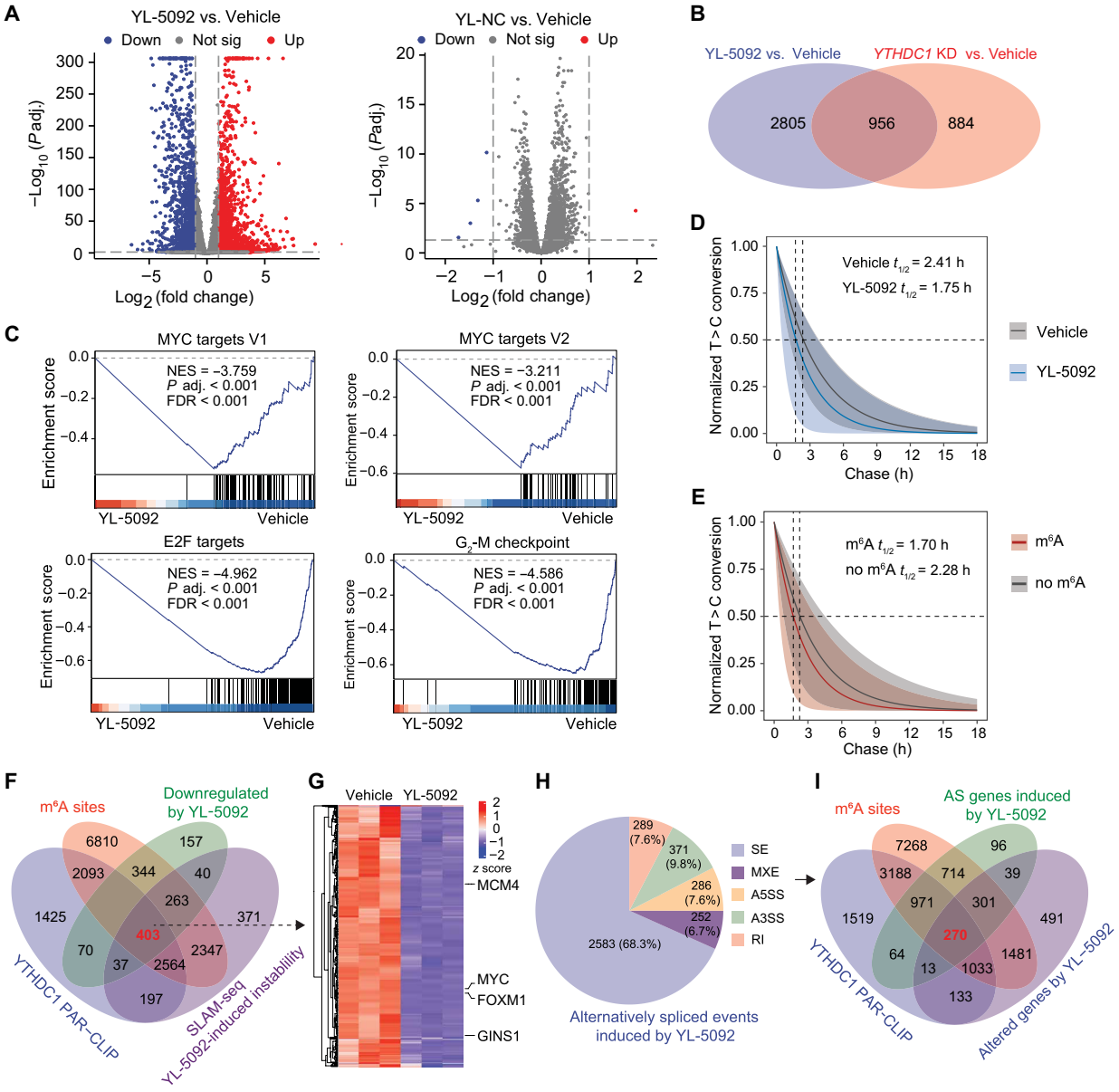

Fig. 3. Global effects of YL-5092 on YTHDC1 targets in AML cells. (**A**) Volcano plots of RNA-seq data showing the up-regulated and down-regulated expression of genes in MOLM-13 cells treated with vehicle, YL-5092 (2 μM), or YL-NC (2 μM) for 72 hours ($n = 3$, independent experiments). The filter condition was twofold change, FDR (false discovery rate) < 0.05. *P* adj., adjusted *P* value. (**B**) Venn diagram depicting the overlap between differentially expressed genes from YL-5092 treatment versus vehicle and published YTHDC1 knockdown versus vehicle RNA-seq datasets. (**C**) Global gene set enrichment analysis (GSEA) enrichment plots showing the top four enriched down-regulated pathways in MOLM-13 cells treated with YL-5092. (**D**) Transcriptome-wide mRNA decay curves for vehicle- and YL-5092–treated MOLM-13 cells. Shaded regions represent the interquartile range (first and third quartiles) for each group ($n = 3$, independent experiments). (**E**) Decay curves of methylated versus non-methylated transcripts in YL-5092–treated MOLM-13 cells. Shaded regions indicate the interquartile range. (**F**) Venn diagram showing overlapping genes among (i) down-regulated genes after YL-5092 treatment (RNA-seq); (ii) m^6A-modified genes (m^6A-seq); (iii) genes with reduced stability upon YL-5092 treatment [thiol(SH)-linked alkylation for the metabolic sequencing of RNA (SLAM-seq)]; and (iv) YTHDC1-binding targets from a published PAR-CLIP dataset. (**G**) Heatmap of expression profiles for the 430 overlapping genes identified in (F), including *MYC*, *FOXM1*, *GINS1*, and *MCM4*. Red and blue shades represent up- and down-regulation, respectively. (**H**) Pie charts showing the distribution of each type of substantially altered splicing events in MOLM-13 cells upon YL-5092 treatment compared with the dimethyl sulfoxide controls. SE, splice exon; MXE, mutually exclusive exons; A5SS, alternative 5′ splice site; A3SS, alternative 3′ splice site; RI, retained intron. (**I**) Venn diagram showing the overlap among YL-5092–dysregulated genes, YL-5092–induced alternatively spliced genes, m^6A-modified genes, and YTHDC1-bound genes from PAR-CLIP.

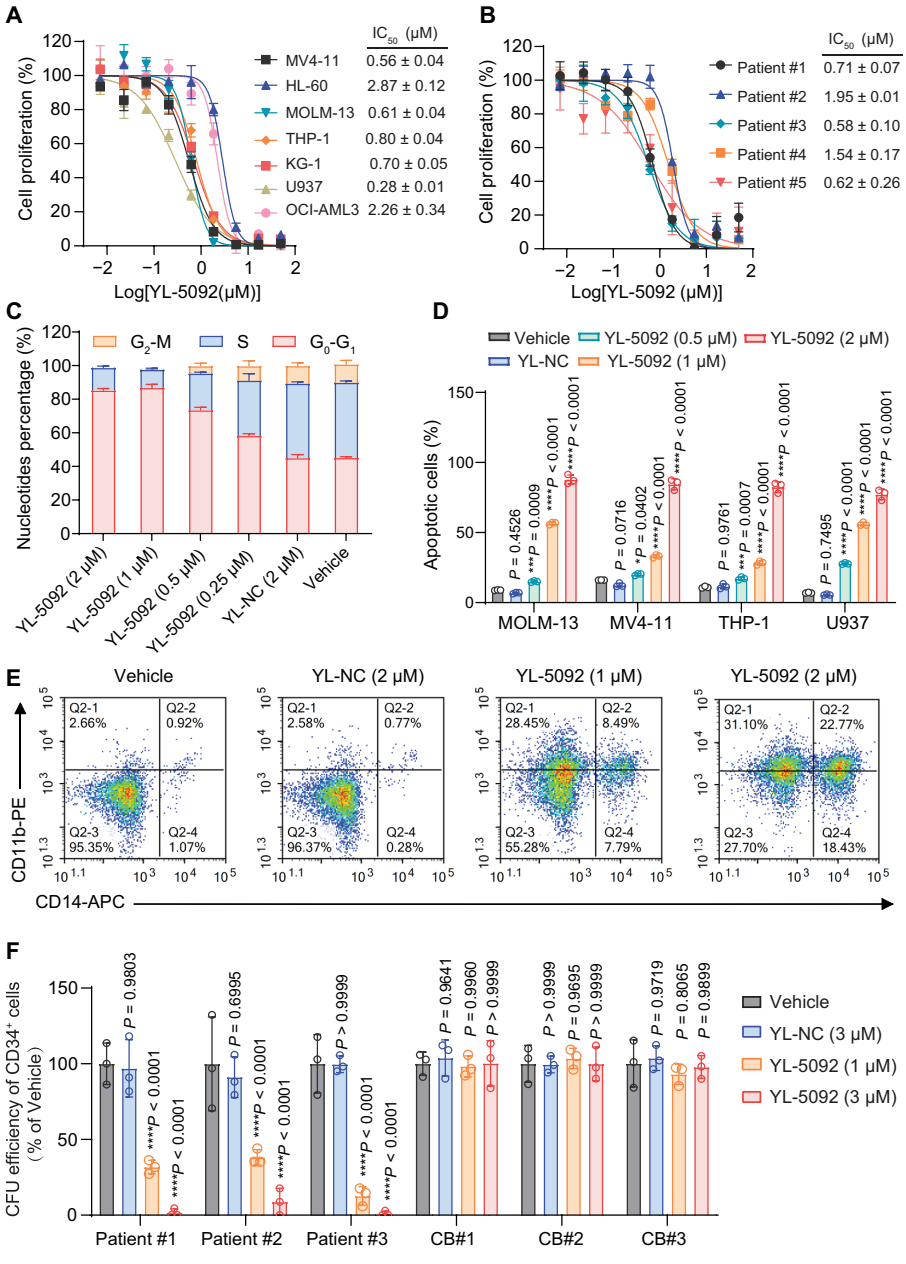

Fig. 4. In vitro anti-AML activity of YL-5092. (**A** and **B**) Growth inhibitory effect of YL-5092 on AML cell lines (A) and primary AML cells derived from patients with AML (B), determined by the methylthiazolyldiphenyl-tetrazolium bromide (MTT) assay ($n = 3$, independent experiments). Cells were treated with YL-5092 at indicated concentrations for 72 hours. (**C**) Cell cycle analysis in MOLM-13 cells treated with YL-5092 or YL-NC at indicated concentrations for 48 hours, analyzed by flow cytometry ($n = 3$, independent experiments). (**D**) Percentage of apoptotic cells in a panel of human AML cell lines after treatment with YL-5092 or YL-NC at the indicated concentrations for 5 days ($n = 3$, independent experiments). (**E**) Effect of 5-day treatment with YL-5092 or YL-NC on the myeloid differentiation in MOLM-13 cells, analyzed by flow cytometry ($n = 3$, independent experiments). (**F**) CFU assay of $CD34^+$ cells from three patients with AML and $CD34^+$ cells from three normal human umbilical CB samples treated with YL-5092 or YL-NC at indicated concentrations for 14 to 16 days ($n = 3$, biological replicates). All data were obtained from three independent experiments. Data are shown as averages ± SD. All data were analyzed using two-way ANOVA compared with the vehicle control group; $^{**}P < 0.01$, $^{***}P < 0.001$, and $^{****}P < 0.0001$. APC, allophycocyanin; PE, phycoerythrin.

the dose-response curve (AUC) as the primary metric. To comprehensively assess YL-5092's activity, specimens were stratified according to (i) fusion gene status, (ii) cytogenetic status (normal karyotype versus abnormal), (iii) clinical risk category, and (iv) mutational status of key driver genes (*KRAS*, *TP53*, *FLT3*, *NPM1*, *DNMT3A*, and *TET2*). As shown in fig. S9, within this cohort of primary samples, we observed no significant differential sensitivity to YL-5092 among these AML subgroup classifications. Furthermore, we evaluated the impact of YL-5092 on the more primitive leukemic and normal hematopoietic progenitor functions. To this end, we performed colony-forming unit (CFU) assays on $CD34^+$-enriched leukemia stem and progenitor cells (LSPCs) versus $CD34^+$-enriched normal hematopoietic stem and progenitor cells (HSPCs). In this assay, YL-5092 markedly inhibited the CFU potential of $CD34^+$ LSPCs from multiple primary human AML specimens but spared $CD34^+$ HSPCs from all umbilical cord blood (CB) samples obtained from healthy donors (Fig. 4F). Moreover, we also tested the effect of YL-5092 on normal hematopoietic lineage differentiation by examining the number and morphology of different types of colonies [burst-forming unit–erythroid (BFU-E), CFU-granulocyte (CFU-G), CFU-macrophage (CFU-M), CFU-granulocyte/macrophage (CFU-GM), and CFU–granulocyte, erythroid, macrophage, megakaryocyte (CFU-GEMM)] derived from CB specimens upon YL-5092 treatment. The result showed that YL-5092 had minimal impact on various types of erythroid and myeloid colonies (figs. S10, A to C). The treatment also did not affect hematopoietic subpopulations as revealed by CD45 and side scatter staining (fig. S10, D and E). Furthermore, we performed secondary CFU plating experiments, and the results showed that both 1- and 3-μM YL-5092–treated groups retained their colony-replating potential equivalent of the vehicle control (fig. S10F). Together, these results suggest that YL-5092 is a potent and selective antileukemia agent with the potential to target the more primitive LSPC compartment while sparing the normal hematopoietic counterparts.

We noticed that knockdown of *YTHDC1* in AML cells reduced its sensitivity to YL-5092 (fig. S11A). This attenuated response was restored upon YTHDC1 overexpression, indicating an on-target inhibitory effect (fig. S11B). Furthermore, YL-5092 was also effective in treating 9 of the 22 solid cancer cell lines we tested along with the

above seven leukemic cell lines (table S5), suggesting the potential utility of YTHDC1 inhibitor beyond leukemia. The protein expression level of YTHDC1 was markedly higher in the YL-5092–sensitive group (seven leukemic and nine solid cancer cell lines) than the YL-5092–resistant group (13 cell lines that did not reach 50% killing at 50 μM YL-5092) (fig. S11, C to G). Moreover, for the 16 cell lines in the YL-5092–sensitive group, the protein expression levels of YTHDC1 substantially correlated with their IC_{50} values of YL-5092 (fig. S11H). Collectively, these data demonstrate that YL-5092 is a potent and selective inhibitor of YTHDC1 in tumor cells.

In vivo activity of YL-5092 in treating AML as a single agent or in combination with venetoclax/azacitidine

Last, we wanted to test the in vivo activity of YL-5092 in treating AML. To this end, we first evaluated the pharmacokinetic (PK) properties of YL-5092 in vivo. When given intraperitoneally (ip; 20 mg/kg) and orally (20 mg/kg), YL-5092 delivered AUC values of 20,035 and 11,083 hours•ng/ml (fig. S12A) and bioavailability at 87.29 and 48.29%, respectively. Intraperitoneal administration was used in subsequent in vivo studies because of superior absorption. The key PK parameters for the intraperitoneal administration with the used dose (70 mg/kg) are summarized here: The AUC and the half-life ($T_{1/2}$) are 161,500 hours•ng/ml and 2.12 hours, respectively. The maximum plasma concentration (C_{max}) is 23,562 ng/ml. Based on the IC_{50}/IC_{90} values from MOLM-13 or U937 cells, a single intraperitoneal of YL-5092 at 70 mg/kg per day maintained the plasma levels at IC_{50} (0.61 μM) or IC_{50} (0.28 μM) and IC_{90} (1.54 μM) or IC_{90} (2.88 μM) for ~16 or 18 hours and 14 or 13 hours, respectively (fig. S12, B and C).

To determine the safety of YL-5092, C57BL/6J mice were administered by intraperitoneal injection of YL-5092 at a dose of 70 mg/kg twice a day for 3 consecutive weeks. There was no overt toxicity and no evident loss of body weight after YL-5092 treatment (fig. S13A). Complete blood count analyses revealed no obvious changes in levels of white blood cells, red blood cells, platelets, hemoglobin, and hematocrit during YL-5092 treatment (fig. S13, B to F). Subsequently, we analyzed bone marrow (BM) samples isolated from mice and observed no significant alterations in the total number of BM cells at different time points during YL-5092 treatment (fig. S13G). We further characterized different hematopoietic cell compartments using flow cytometric analysis (fig. S13H). It was found that YL-5092 treatment did not result in significant changes in the relative numbers of stem cell–enriched $Lin^-Sca\text{-}1^+c\text{-}Kit^+$ (LSK) cells (fig. S13I). Among LSK cells, there were no significant changes in the relative proportions of phenotypically defined long-term HSCs ($Lin^-Sca\text{-}1^+c\text{-}Kit^+CD150^+CD48^-$; fig. S13J), multipotent progenitors ($Lin^-Sca\text{-}1^+c\text{-}Kit^+CD150^-CD48^-$; fig. S13K), and downstream hematopoietic progenitor cell subsets (HPC-1, $Lin^-Sca\text{-}1^+c\text{-}Kit^+CD150^-CD48^+$; HPC-2, $Lin^-Sca\text{-}1^+$ $c\text{-}Kit^+CD150^+CD48^+$; fig. S13, L and M). In addition, YL-5092 treatment did not significantly affect the myeloerythroid progenitor–enriched LKS^- population ($Lin^-c\text{-}Kit^+Sca\text{-}1^-$; fig. S13N) or the granulocyte-macrophage progenitor-enriched population ($Lin^-Sca\text{-}1^-c\text{-}Kit^+CD41^-CD150^-CD16/32^+$; fig. S13O). Furthermore, we analyzed differentiated cell populations in the BM and observed no significant changes in their relative numbers during YL-5092 treatment, including myeloid cells ($Mac1^+Gr1^+$; fig. S13P), $CD4^+$ or $CD8^+$ T cells (fig. S13, Q and R), mature recirculating B cells ($B220^+CD19^+CD93^-$; fig. S13S), and developing B cells ($B220^+CD19^+CD93^+$; fig. S13T). To explore the effects of YL-5092 on the function of other tissues, we measured serum biochemicals such as alanine aminotransferase, aspartate aminotransferase, creatinine, uric acid, and α-hydroxybutyrate dehydrogenase at various time points during YL-5092 treatment. We found that mice in the YL-5092 treatment group exhibited no significant differences in these serum biochemical compared to the vehicle controls, indicating that YL-5092 (70 mg/kg) had no obvious toxicity on heart, liver, or kidney function (fig. S14, A to E). Further histological analysis of the heart, liver, spleen, lung, and kidney by hematoxylin and eosin (H&E) staining revealed no obvious abnormalities in YL-5092–treated mice (fig. S14F). Together, YL-5092 was well tolerated and did not result in obvious adverse events in mice, suggesting that YL-5092 is a safe antileukemia agent.

Subsequently, we assessed the in vivo antileukemia activity of YL-5092 in cell line–derived xenograft (CDX) or patient-derived xenograft (PDX) models of AML. MOLM-13 or U937 leukemic cells expressing luciferase were used to generate CDX models of AML. Treatment with YL-5092 [70 mg/kg, ip, twice per day (b.i.d.)] or vehicle was initiated 4 days after cell transplantation and was continued for 18 consecutive days with the progression of disease monitored by luciferase imaging in the two CDX models (Fig. 5A). No weight loss was observed during the treatment (fig. S15, A and B). Compared with the control group, YL-5092 treatment substantially alleviated the progression of leukemia and markedly prolonged the overall survival of the treated mice (Fig. 5, B to E, and fig. S15, C and D). As determined by flow cytometry analysis, YL-5092 treatment substantially reduced leukemia burden in the BM, peripheral blood, and spleens of the mice (Fig. 5, F to H, and fig. S15E). H&E and immunohistochemical staining of the spleen confirmed less dissemination of AML cells in YL-5092–treated mice (Fig. 5I). We performed gene expression analysis on leukemic cells isolated from the BM of YL-5092–treated mice and found that YL-5092 treatment profoundly reduced the expression of YTHDC1 target genes, including *MYC*, *FOXM1*, *GINS1*, *MCM2*, *MCM4*, and *MCM5* (Fig. 5J), indicating an on-target effect of YL-5092 in vivo.

Next, we tested the therapeutic efficacy of YL-5092 in PDX models of AML representing complex genetic heterogeneity of the human AML disease. Specifically, we generated four PDX models from four independent specimens from patients with AML containing various combinations of oncogenic mutations in *TET2*, *FLT3*, *NPM1*, *NRAS*, *PTPN11*, and others, commonly reported in human AML (table S3). Primary AML cells were xenografted into NSG-SGM3 mice pretreated with busulfan. When recipient mice had successfully engrafted AML cells in the BM, the mice were treated with YL-5092 or vehicle for 21 days (Fig. 6A). During the experiment, no weight loss was observed (fig. S15, F to I), and YL-5092 treatment substantially decreased leukemia burden in the BM compared with the control group across all four PDX models tested (Fig. 6, B to F) and substantially prolonged the overall survival of the treated PDX-4 mice (Fig. 6G). We next also wanted to assess the efficacy of YL-5092 on LSCs in vivo. To this end, we serially transplanted the BM cells harvested from primary xenografts treated with vehicle or YL-5092 into secondary recipients. Serial transplantation is a functional test of LSCs when studying genetic and pharmacological perturbations (*38*, *39*). At the end point, the mice that received the YL-5092–treated BM samples demonstrated a marked loss in leukemia reconstitution capacity compared with the vehicle control, indicating that YL-5092 had markedly impaired the LSC compartment required to drive long-term leukemic propagation (Fig. 6, H to K). Together, these results

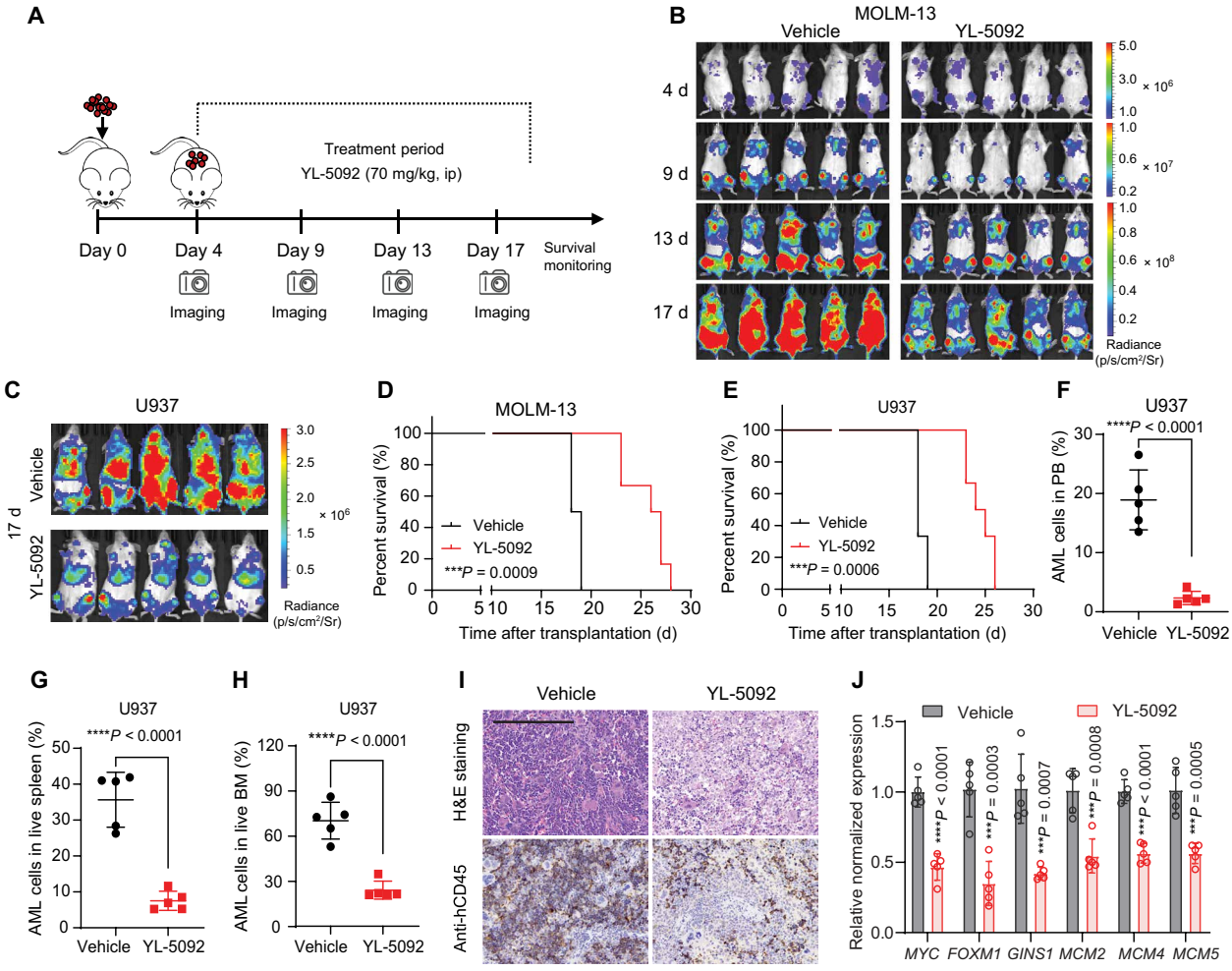

Fig. 5. Treatment with YL-5092 inhibits leukemogenesis. (**A**) Schematic of the MOLM-13 and U937 xeno-transplantation model and treatment workflow. Treatment with vehicle or YL-5092 (70 mg/kg, ip, b.i.d.) was initiated 4 days after transplantation and lasted for 18 days. (**B** and **C**) Bioluminescence imaging of MOLM-13 (B) and U937(C) xeno-transplanted mice treated with vehicle or YL-5092, taken on days 4, 9, 13, and 17 ($n = 5$, biological replicates). (**D** and **E**) Kaplan-Meier survival curves of MOLM-13 (D) and U937(E) xeno-transplanted mice treated with vehicle or YL-5092 ($n = 6$, biological replicates). (**F** to **H**) Percentage of hCD45 and hCD33 double-positive cells (leukemia cells) in the peripheral blood (F), spleen (G), and BM (H) of U937 xeno-transplanted mice after treatment with vehicle or YL-5092 (70 mg/kg). Data are presented as averages ± SD of five biological replicates. (**I**) Representative H&E staining and immunohistochemical staining of spleens of U937 xeno-transplanted mice on day 17 after transplant. Scale bar, 200 μm. $n = 5$, biological replicates. (**J**) Relative expression levels of *MYC*, *FOXM1*, *GINS1*, *MCM2*, *MCM4*, and *MCM5* in the BM-derived mononuclear cells of U937 xeno-transplanted mice on day 17 after transplant. Data are presented as averages ± SD of four technical replicates from five biological replicate experiments. Statistical differences were determined by log-rank (Mantel-Cox) test [(D) and (E)], unpaired two-tailed Student's *t* test [(F) to (H)], or multiple *t* tests (J). ***$P < 0.001$ and ****$P < 0.0001$.

demonstrate that the pharmacological inhibition of YTHDC1 by YL-5092 substantially suppresses leukemia progression and impairs functional LSCs from genetically heterogeneous primary AML specimens in vivo.

Despite the excellent performance of YL-5092 in treating human AML as a single agent, we propose that future development of YTHDC1 inhibitors in the AML clinic will inevitably need to test its therapeutic potential in combination with standard AML therapies, given the complex disease heterogeneity of human AML. To this end, we next examined the ability of YL-5092 in combination with the widely used AML therapy venetoclax plus azacitidine (Ven/Aza) (*35*, *40*). We found that YL-5092 exhibited a strong synergistic effect with the small-molecule selective B cell lymphoma-2 (BCL-2) inhibitor venetoclax in treating AML cell line MOLM-13 cells in vitro (Fig. 7, A and B). To investigate the combinatorial mechanism, we performed RNA-seq analysis on MOLM-13 AML cells under four conditions: control, YL-5092, Ven/Aza, and combination. The unsupervised clustering of differentially expressed genes (data file S1) revealed nine distinct expression patterns (fig. S16A). Clusters 2 and 4 exhibited genes up-regulated/sustained by Ven/Aza but suppressed by YL-5092 or combination (fig. S16B), suggesting that these genes may mediate resistance to Ven/Aza that is counteracted by YL-5092. The pathway analysis of clusters 2 and 4 highlighted enrichment for known Ven resistance pathways, including oxidative phosphorylation, electron transport chain complexes, and a previously reported Ven resistance gene signature (fig. S16C) (*41*). This aligns with established literature linking Ven resistance to mitochondrial biology (*42*, *43*). Thus, YL-5092 may enhance

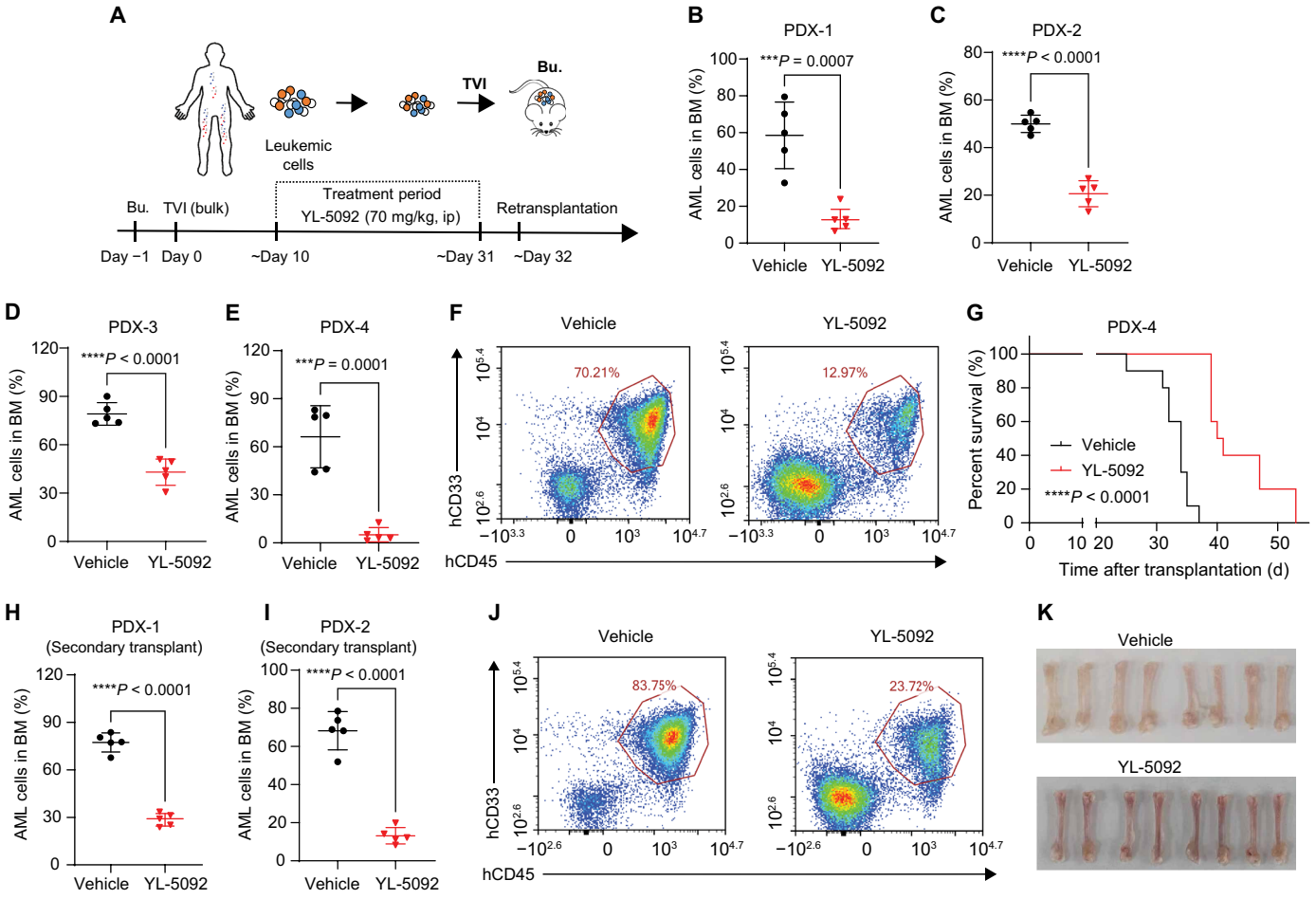

Fig. 6. Single-agent activity of YL-5092 in PDX mouse models. (**A**) Schematic of the patient-derived xeno-transplantation AML mouse model. Treatment with vehicle or YL-5092 (70 mg/kg, ip, b.i.d.) was initiated 10 days after transplantation and lasted for 21 days. (**B** to **E**) Flow cytometric quantification of patient AML (human $CD45^+CD33^+$) cells in the BM from PDX-1 (B), PDX-2 (C), PDX-3 (D), and PDX-4 (E) mice after the 21-day full treatment ($n = 5$, biological replicates). (**F**) Representative flow cytometric plots of patient-derived AML cells in the BM from PDX-1 are shown, as related to (B). $n = 5$, biological replicates. (**G**) Kaplan-Meier survival curves of AML PDX mouse model (PDX4) treated with YL-5092 ($n = 10$, biological replicates). (**H** and **I**) Flow cytometric quantification of patient AML (human $CD45^+CD33^+$) cells in the BM from the secondarily transplanted PDX-1 (H) and PDX-2 (I) mice 30 days posttransplantation ($n = 5$, biological replicates). (**J** and **K**) Representative flow cytometric plots (J) and mouse femur images (K) from the secondarily transplanted PDX-1 are shown, as related to (H). $n = 5$, biological replicates. All data are presented as averages ± SD. Statistical differences were determined by log-rank (Mantel-Cox) test (G) and unpaired two-tailed Student's *t* test [(B) to (E) and (H) and (I)]. ***$P < 0.001$ and ****$P < 0.0001$. TVI, tail vein injection; BU., busulfan.

Ven/Aza efficacy by suppressing these resistance-associated pathways. We next assessed the efficacy of Ven/Aza + YL-5092 across different AML subtypes. The analysis of primary AML specimens with different fusion gene status, cytogenetic profile, clinical risk category, and mutational status of key driver genes (*KRAS*, *TP53*, *FLT3*, *NPM1*, *DNMT3A*, and *TET2*) revealed no significant differential sensitivity to the combination therapy (fig. S17), suggesting that YL-5092 could be broadly effective in primary AML. Subsequently, we tested YL-5092 at a lower dose of 50 mg/kg and a shorter treatment time in combination with standard AML therapy Ven/Aza in CDX and PDX models of human AML. As shown in Fig. 7 (C to F), YL-5092 or Ven/Aza treatment alone decreased leukemic burden and extended survival of the recipient mice to a degree, and the YL-5092 + Ven/Aza combination exhibited an even stronger antileukemia effect and extension of survival compared with the single arms. Similarly, combined treatment on the PDX model can also reduce the leukemia burden in the BM of mice and prolong their survival time (Fig. 7, G to I).

Last, we evaluated the impact of YL-5092 on normal hematopoietic stem/progenitor cell functions to address the potential concern about its toxicity toward the hematopoietic system. To this end, we extensively treated human CB-engrafted mice with 3 weeks of YL-5092 (70 mg/kg) or vehicle control. We observed that treatment of YL-5092 did not reduce the total engraftment potential of two independent CB specimens compared to the vehicle group (fig. S18, A and B). Besides, YL-5092 treatment also did not impair the percentage of differentiated $CD15^+$ granulocytes, $CD14^+$ monocytes, and $CD3^+$ lymphocytes or the more primitive $CD34^+$ HSPCs and $CD38^+$ progenitor cells (figs. S18C). In addition, we assessed the impact of YL-5092 on HSC self-renewal via an alternative functional assay, where we first treated a CB specimen with YL-5092 in a culture dish and then engrafted the treated specimen in immunodeficient mice. This experiment could directly test whether YL-5092 had

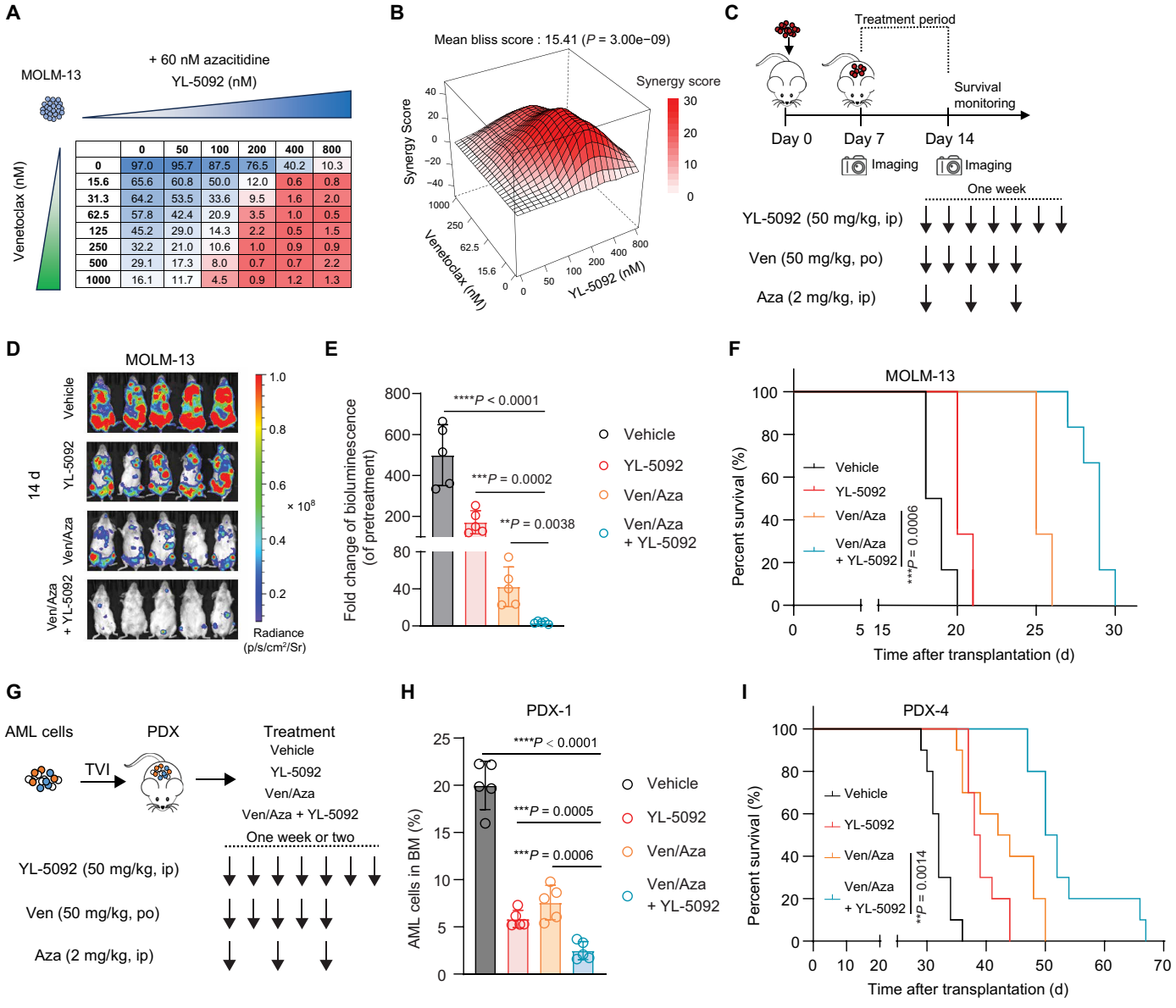

	0	50	100	200	400	800
0	97.0	95.7	87.5	76.5	40.2	10.3
15.6	65.6	60.8	50.0	12.0	0.6	0.8
31.3	64.2	53.5	33.6	9.5	1.6	2.0
62.5	57.8	42.4	20.9	3.5	1.0	0.5
125	45.2	29.0	14.3	2.2	0.5	1.5
250	32.2	21.0	10.6	1.0	0.9	0.9
500	29.1	17.3	8.0	0.7	0.7	2.2
1000	16.1	11.7	4.5	0.9	1.2	1.3

Fig. 7. Therapeutic efficacy of YL-5092 combined with Ven/Aza. (**A**) Viability of MOLM-13 cells treated with YL-5092 + Ven/Aza at various dose combinations. Numbers indicate mean viability. Data are presented as averages of three technical replicates from three independent experiments. (**B**) Heat map showing the Bliss synergy scores of synergies for YL-5092 in combination with venetoclax at fixed dose combinations in MOLM-13 cells. (**C**) A diagram depicting workflow and design of the regimens used for in vivo treatment. (**D**) Bioluminescence imaging of MOLM-13 xeno-transplanted mice treated with YL-5092, Ven/Aza, or triple-drug combination, taken on day 14 ($n = 5$, biological replicates). (**E**) Quantification of bioluminescence signal for MOLM-13 xeno-transplanted mice after treatment with YL-5092, Ven/Aza, or triple-drug combination ($n = 5$, biological replicates). Data are presented as averages ± SD. (**F**) Kaplan-Meier survival curves of MOLM-13 xeno-transplanted mice treated with YL-5092, Ven/Aza, or triple-drug combination ($n = 6$, biological replicates). (**G**) Diagram depicting workflow and design of the regimens used for in vivo treatment. (**H**) Impact of in vivo YL-5092, Ven/Aza, or triple-drug combination treatments on the BM tumor burden of PDX ($n = 5$, biological replicates). Data are presented as averages ±SD. (**I**) Kaplan-Meier survival curves of AML PDX mouse model (PDX-4) treated with YL-5092, Ven/Aza, or triple-drug combination ($n = 10$, biological replicates). Statistical differences were determined by unpaired two-tailed Student's *t* test [(E) and (H)] and log-rank (Mantel-Cox) test [(F) and (I)]. $^{**}P < 0.01$, $^{***}P < 0.001$, and $^{****}P < 0.0001$.

impaired the self-renewing HSC subcompartment. Our results showed that both 1 and 3 μM YL-5092 had negligible impact on the final engraftment of the normal HSCs (fig. S18D). Similarly, we observed that the combination of YL-5092 and Ven/Aza also had no substantial impact on the engraftment and lineage reconstitution function of hematopoietic stem/progenitor cells (fig. S18E). In summary, these data demonstrate a promising preclinical potential of YL-5092 in treating human AML both as a single agent and in combination with venetoclax-based therapies without overt toxicity toward the normal hematopoietic system.

DISCUSSION

RNA modifications are widespread in various RNA types and have emerged as a key regulatory mechanism in posttranscriptional

control of gene expression. Recent years have witnessed a burst of interest in understanding of the RNA modification biology that is often referred to as epitranscriptomics (*44*, *45*). Currently, more than 170 distinct RNA modifications on cellular RNA have been identified (*46*). The RNA m^6A modification is the most abundant modification of RNA in eukaryotic cells and is essential for multiple physiological processes (*1*, *2*, *45*, *47*). The malfunctions of the cellular machinery regulating the m^6A modification—including writers (*48*), erasers (*3*, *49*, *50*), and readers (*10*–*18*, *51*–*56*)—have been linked to pathologies such as cancer (*57*, *58*), obesity (*59*–*61*), and neurodegeneration (*25*, *62*). Therefore, the m^6A modification machinery has recently attracted great attention from the drug discovery community. Recent advances in epitranscriptomic drug finding have yielded multiple potent small-molecule inhibitors targeting m^6A regulatory proteins, including methyltransferase-like protein 3 (METTL3), fat mass and obesity-associated protein (FTO) demethylase, YTHDF2, and IGF2BP2 readers, demonstrating promising therapeutical potential for related disease treatment (*49*, *63*–*69*). Despite these developments, the pharmacological targeting landscape remains incomplete, given that no potent YTHDC1 inhibitors with validated in vivo efficacy have been reported to date. Whether small molecules targeting YTHDC1 have therapeutical potential against related diseases remains unknown. We here report YL-5092 as a first-in-class inhibitor of m^6A reader YTHDC1 and demonstrate its promising therapeutic potential in treating human AML.

YL-5092, as reported here, is a highly potent and selective YTHDC1 inhibitor with a single-digit nanomolar potency ($IC_{50} = 7.4$ nM), which was found through structure-guided stepwise optimization toward a hit compound (Hit-1). The potency and selectivity of YL-5092 were well explained by the x-ray crystal structure of the YTHDC1–YL-5092 complex. We demonstrated the target engagement of YL-5092 in living leukemic cells and showed that this compound decreased the stability of the mRNA targets of YTHDC1. YL-5092 also evidently suppressed the LLPS mediated by YTHDC1, which is critical for executing the biological function of YTHDC1. Of importance is that YL-5092 potently induced cell death in various AML cell lines and primary AML specimens. Our results support the previous findings that YTHDC1 is overexpressed in AML and is required for the survival of human AML cells. In addition, it is worth mentioning that YL-5092 may also be effective in treating some solid tumor types where YTHDC1 is essential.

YL-5092 displayed potent in vivo antileukemic activity in xenograft models derived from multiple AML cell lines and specimens of patients with primary AML of complex disease heterogeneity. To assess the impact of YTHDC1 inhibition on LSC function, we performed secondary transplantation assays to evaluate residual LSC activity in primary xenografts treated in vivo with YL-5092. The results demonstrated substantially reduced engraftment potential in secondary recipients, indicating impairment of the LSC compartment by YL-5092. These findings align with prior studies establishing YTHDC1's role in LSC maintenance (*12*). Although these data robustly demonstrate functional LSC suppression, future studies using limiting dilution assays could provide more precise quantification of the fold of reduction in LSC frequency. Moreover, a lower dosage of YL-5092 combined with Ven/Aza, a newly approved standard care for patients with AML in clinical practice, showed excellent combinatorial therapeutic efficacy in both CDX and PDX models. Furthermore, we propose that future studies should thoroughly characterize the potential mechanisms underlying the YL-5092 and Ven/Aza combination therapy in AML and identify AML subtypes sensitive to this regimen.

This study has some limitations. First, our current studies have not identified a specific AML subtype exhibiting heightened sensitivity to YL-5092. We will use a broader panel of primary patient samples in future investigations. This expanded analysis aims to delineate YL-5092–sensitive AML subtypes, thereby providing a foundation for the precise treatment of AML. Second, although we have undertaken preliminary safety studies, our research into the safety profile of YL-5092 is still insufficient. Our existing data indicate that YL-5092 had no obvious toxicity at the therapeutically effective dose in mice. Previous studies have shown that, although YTHDC1 is required for the survival and self-renewal of both LSCs and HSPCs, YTHDC1 haploinsufficiency only reduces the self-renewal of LSCs but not HSPCs in vivo (*12*). This differential sensitivity likely stems from the greater reliance of AML cells, which frequently overexpress YTHDC1, on YTHDC1 function compared with normal HSPCs. This provides a theoretical basis for achieving a therapeutic window using YL-5092 to target AML while sparing normal hematopoiesis. Consistent with these results, YL-5092 at the desired dose could efficiently impair functional LSCs while sparing normal HSPCs, demonstrating a favorable therapeutic window for leukemia treatment. Nonetheless, the clinical safety of YL-5092 still needs to be thoroughly investigated in future studies.

In summary, we have identified a highly potent and selective first-in-class YTHDC1 inhibitor and have demonstrated its strong antileukemic activity toward human AML while largely sparing normal hematopoiesis. This compound, used alone or in combination with the newly approved standard care of AML (Ven/Aza), demonstrates potent in vivo antileukemic activity, providing the proof of principle that targeting YTHDCl is a promising strategy for leukemia treatment.

MATERIALS AND METHODS

Study design

The primary objective of this study was to identify a potent and selective small-molecule inhibitor of YTHDC1 and examine its anti-AML activity and impact on normal hematopoietic cells. We initially identified a hit compound, Hit-1, via FP-based screening. The crystal structure of the Hit-1 complex was determined by x-ray crystallography, which informed a structure-based optimization strategy leading to the highly active compound YL-5092. This compound was extensively characterized through a series of in vitro and in vivo assays, including DSF, SPR, CETSA, FRAP, qPCR, RIP-qPCR, RNA-seq, and SLAM-seq, as well as assessments of cell proliferation, cell cycle progression, apoptosis, and differentiation. In vivo studies included PK profiling and efficacy evaluations in CDX and PDX models of human AML. To ensure experimental reproducibility, mice were randomly assigned to groups. Although the experiments were not conducted in a blinded manner, each study included multiple animals ($n = 5$ to 10 per group). Statistical methods and experimental replicates are detailed in the respective figure legends, and a complete description of materials and methods is available in the Supplementary Materials.

Statistical analysis

All data were analyzed with GraphPad Prism 8.0 software. Statistical comparison between different groups was performed by one-way

or two-way analysis of variance (ANOVA), unpaired two-tailed Student's *t* test, multiple *t* tests, or log-rank (Mantel-Cox) test. Differences were considered statistically significant when $P < 0.05$, $*P < 0.05$, $**P < 0.01$, $***P < 0.001$, and $****P < 0.0001$.

Supplementary Materials

The PDF file includes:
Materials and Methods
Figs. S1 to S18
Tables S1 to S5
Spectral data for compounds
NMR spectra of all compounds
HRMS spectra of all compounds
References (*70*–*76*)

Other Supplementary Material for this manuscript includes the following:
Data files S1 and S2
MDAR Reproducibility Checklist

REFERENCES AND NOTES

1. K. D. Meyer, Y. Saletore, P. Zumbo, O. Elemento, C. E. Mason, S. R. Jaffrey, Comprehensive analysis of mRNA methylation reveals enrichment in 3′ UTRs and near stop codons. *Cell* **149**, 1635–1646 (2012).
2. P. C. He, C. He, m^{6}A RNA methylation: From mechanisms to therapeutic potential. *EMBO J.* **40**, e105977 (2021).
3. G. Jia, Y. Fu, X. Zhao, Q. Dai, G. Zheng, Y. Yang, C. Yi, T. Lindahl, T. Pan, Y. G. Yang, C. He, N6-methyladenosine in nuclear RNA is a major substrate of the obesity-associated FTO. *Nat. Chem. Biol.* **7**, 885–887 (2011).
4. Y. Fu, D. Dominissini, G. Rechavi, C. He, Gene expression regulation mediated through reversible m^{6}A RNA methylation. *Nat. Rev. Genet.* **15**, 293–306 (2014).
5. Y. Zhao, Y. Shi, H. Shen, W. Xie, m^{6}A-binding proteins: The emerging crucial performers in epigenetics. *J. Hematol. Oncol.* **13**, 35 (2020).
6. D. P. Patil, B. F. Pickering, S. R. Jaffrey, Reading m^{6}A in the transcriptome: m^{6}A-binding proteins. *Trends Cell Biol.* **28**, 113–127 (2018).
7. R. Shi, S. Ying, Y. Li, L. Zhu, X. Wang, H. Jin, Linking the YTH domain to cancer: The importance of YTH family proteins in epigenetics. *Cell Death Dis.* **12**, 346 (2021).
8. C. R. Alarcón, H. Goodarzi, H. Lee, X. Liu, S. Tavazoie, S. F. Tavazoie, HNRNPA2B1 is a mediator of m^{6}A-dependent nuclear RNA processing events. *Cell* **162**, 1299–1308 (2015).
9. H. Huang, H. Weng, W. Sun, X. Qin, H. Shi, H. Wu, B. S. Zhao, A. Mesquita, C. Liu, C. L. Yuan, Y. C. Hu, S. Hüttelmaier, J. R. Skibbe, R. Su, X. Deng, L. Dong, M. Sun, C. Li, S. Nachtergaele, Y. Wang, C. Hu, K. Ferchen, K. D. Greis, X. Jiang, M. Wei, L. Qu, J. L. Guan, C. He, J. Yang, J. Chen, Recognition of RNA N^6-methyladenosine by IGF2BP proteins enhances mRNA stability and translation. *Nat. Cell Biol.* **20**, 285–295 (2018).
10. J. Paris, M. Morgan, J. Campos, G. J. Spencer, A. Shmakova, I. Ivanova, C. Mapperley, H. Lawson, D. A. Wotherspoon, C. Sepulveda, M. Vukovic, L. Allen, A. Sarapuu, A. Tavosanis, A. V. Guitart, A. Villacreces, C. Much, J. Choe, A. Azar, L. N. van de Lagemaat, D. Vernimmen, A. Nehme, F. Mazurier, T. C. P. Somervaille, R. I. Gregory, D. O'Carroll, K. R. Kranc, Targeting the RNA m^{6}A reader YTHDF2 selectively compromises cancer stem cells in acute myeloid leukemia. *Cell Stem Cell* **25**, 137–148.e6 (2019).
11. H. Wang, H. Zuo, J. Liu, F. Wen, Y. Gao, X. Zhu, B. Liu, F. Xiao, W. Wang, G. Huang, B. Shen, Z. Ju, Loss of YTHDF2-mediated m^{6}A-dependent mRNA clearance facilitates hematopoietic stem cell regeneration. *Cell Res.* **28**, 1035–1038 (2018).
12. Y. Sheng, J. Wei, F. Yu, H. Xu, C. Yu, Q. Wu, Y. Liu, L. Li, X. L. Cui, X. Gu, B. Shen, W. Li, Y. Huang, S. Bhaduri-McIntosh, C. He, Z. Qian, A critical role of nuclear m6A reader YTHDC1 in leukemogenesis by regulating MCM complex-mediated DNA replication. *Blood* **138**, 2838–2852 (2021).
13. Y. Cheng, W. Xie, B. F. Pickering, K. L. Chu, A. M. Savino, X. Yang, H. Luo, D. T. Nguyen, S. Mo, E. Barin, A. Velleca, T. M. Rohwetter, D. J. Patel, S. R. Jaffrey, M. G. Kharas, N6-methyladenosine on mRNA facilitates a phase-separated nuclear body that suppresses myeloid leukemic differentiation. *Cancer Cell* **39**, 958–972.e8 (2021).
14. H. Weng, F. Huang, Z. Yu, Z. Chen, E. Prince, Y. Kang, K. Zhou, W. Li, J. Hu, C. Fu, T. Aziz, H. Li, J. Li, Y. Yang, L. Han, S. Zhang, Y. Ma, M. Sun, H. Wu, Z. Zhang, M. Wunderlich, S. Robinson, D. Braas, J. T. Hoeve, B. Zhang, G. Marcucci, J. C. Mulloy, K. Zhou, H. F. Tao, X. Deng, D. Horne, M. Wei, H. Huang, J. Chen, The m^{6}A reader IGF2BP2 regulates glutamine metabolism and represents a therapeutic target in acute myeloid leukemia. *Cancer Cell* **40**, 1566–1582.e10 (2022).
15. Y. G. Hong, Z. Yang, Y. Chen, T. Liu, Y. Zheng, C. Zhou, G. C. Wu, Y. Chen, J. Xia, R. Wen, W. Liu, Y. Zhao, J. Chen, X. Gao, Z. Chen, The RNA m^{6}A reader YTHDF1 is required for acute myeloid leukemia progression. *Cancer Res.* **83**, 845–860 (2023).
16. Z. Li, P. Qian, W. Shao, H. Shi, X. C. He, M. Gogol, Z. Yu, Y. Wang, M. Qi, Y. Zhu, J. M. Perry, K. Zhang, F. Tao, K. Zhou, D. Hu, Y. Han, C. Zhao, R. Alexander, H. Xu, S. Chen, A. Peak, K. Hall, M. Peterson, A. Perera, J. S. Haug, T. Parmely, H. Li, B. Shen, J. Zeitlinger, C. He, L. Li, Suppression of m^{6}A reader Ythdf2 promotes hematopoietic stem cell expansion. *Cell Res.* **28**, 904–917 (2018).
17. N. Zhang, Y. Shen, H. Li, Y. Chen, P. Zhang, S. Lou, J. Deng, The m6A reader IGF2BP3 promotes acute myeloid leukemia progression by enhancing RCC2 stability. *Exp. Mol. Med.* **54**, 194–205 (2022).
18. J. Fan, M. Zhuang, W. Fan, M. Hou, RNA N6-methyladenosine reader IGF2BP3 promotes acute myeloid leukemia progression by controlling stabilization of EPOR mRNA. *PeerJ* **11**, e15706 (2023).
19. M. Hirschfeld, B. Zhang, M. Jaeger, S. Stamm, T. Erbes, S. Mayer, X. Tong, E. Stickeler, Hypoxia-dependent mRNA expression pattern of splicing factor YT521 and its impact on oncological important target gene expression. *Mol. Carcinog.* **53**, 883–892 (2014).
20. B. Zhang, X. Shao, J. Zhou, J. Qiu, Y. Wu, J. Cheng, YT521 promotes metastases of endometrial cancer by differential splicing of vascular endothelial growth factor A. *Tumour Biol.* **37**, 15543–15549 (2016).
21. J. Widagdo, V. Anggono, J. J. Wong, The multifaceted effects of YTHDC1-mediated nuclear m^{6}A recognition. *Trends Genet.* **38**, 325–332 (2022).
22. S. D. Kasowitz, J. Ma, S. J. Anderson, N. A. Leu, Y. Xu, B. D. Gregory, R. M. Schultz, P. J. Wang, Nuclear m^{6}A reader YTHDC1 regulates alternative polyadenylation and splicing during mouse oocyte development. *PLOS Genet.* **14**, e1007412 (2018).
23. W. Xiao, S. Adhikari, U. Dahal, Y. S. Chen, Y. J. Hao, B. F. Sun, H. Y. Sun, A. Li, X. L. Ping, W. Y. Lai, X. Wang, H. L. Ma, C. M. Huang, Y. Yang, N. Huang, G. B. Jiang, H. L. Wang, Q. Zhou, X. J. Wang, Y. L. Zhao, Y. G. Yang, Nuclear m^{6}A reader YTHDC1 regulates mRNA splicing. *Mol. Cell* **61**, 507–519 (2016).
24. I. A. Roundtree, G. Z. Luo, Z. Zhang, X. Wang, T. Zhou, Y. Cui, J. Sha, X. Huang, L. Guerrero, P. Xie, E. He, B. Shen, C. He, YTHDC1 mediates nuclear export of N^6-methyladenosine methylated mRNAs. *eLife* **6**, e31311 (2017).
25. F. Li, Y. Yi, Y. Miao, W. Long, T. Long, S. Chen, W. Cheng, C. Zou, Y. Zheng, X. Wu, J. Ding, K. Zhu, D. Chen, Q. Xu, J. Wang, Q. Liu, F. Zhi, J. Ren, Q. Cao, W. Zhao, N^6-methyladenosine modulates nonsense-mediated mRNA decay in human glioblastoma. *Cancer Res.* **79**, 5785–5798 (2019).
26. Z. Zhang, Q. Wang, X. Zhao, L. Shao, G. Liu, X. Zheng, L. Xie, Y. Zhang, C. Sun, R. Xu, YTHDC1 mitigates ischemic stroke by promoting Akt phosphorylation through destabilizing *PTEN* mRNA. *Cell Death Dis.* **11**, 977 (2020).
27. H. Yan, L. Zhang, X. Cui, S. Zheng, R. Li, Roles and mechanisms of the m^{6}A reader YTHDC1 in biological processes and diseases. *Cell Death Discov.* **8**, 237 (2022).
28. Z.-H. Chen, T.-Q. Chen, Z.-C. Zeng, D. Wang, C. Han, Y.-M. Sun, W. Huang, L.-Y. Sun, K. Fang, Y.-Q. Chen, X.-Q. Luo, W.-T. Wang, Nuclear export of chimeric mRNAs depends on an lncRNA-triggered autoregulatory loop in blood malignancies. *Cell Death Dis.* **11**, 566 (2020).
29. R. K. Bedi, D. Huang, L. Wiedmer, Y. Li, A. Dolbois, J. A. Wojdyla, M. E. Sharpe, A. Caflisch, P. Sledz, Selectively disrupting m^{6}A-dependent protein-RNA interactions with fragments. *ACS Chem. Biol.* **15**, 618–625 (2020).
30. Y. Li, R. K. Bedi, F. Nai, V. von Roten, A. Dolbois, F. Zálešák, R. Nachawati, D. Huang, A. Caflisch, Structure-based design of ligands of the m^{6}A-RNA reader YTHDC1. *Eur. J. Med. Chem. Rep.* **5**, 100057 (2022).
31. F. Nai, R. Nachawati, F. Zálešák, X. Wang, Y. Li, A. Caflisch, Fragment Ligands of the m(6) A-RNA Reader YTHDF2. *ACS Med. Chem. Lett.* **13**, 1500–1509 (2022).
32. S. M. Myers, D. C. Miller, L. Molyneux, M. Arasta, R. H. Bawn, T. J. Blackburn, S. J. Cook, N. Edwards, J. A. Endicott, B. T. Golding, R. J. Griffin, T. Hammonds, I. R. Hardcastle, S. J. Harnor, A. B. Heptinstall, P. A. Lochhead, M. P. Martin, N. C. Martin, D. R. Newell, P. J. Owen, L. C. Pang, T. Reuillon, L. J. M. Rigoreau, H. D. Thomas, J. A. Tucker, L. Z. Wang, A. C. Wong, M. E. M. Noble, S. R. Wedge, C. Cano, Identification of a novel orally bioavailable ERK5 inhibitor with selectivity over p38α and BRD4. *Eur. J. Med. Chem.* **178**, 530–543 (2019).
33. C. Xu, X. Wang, K. Liu, I. A. Roundtree, W. Tempel, Y. Li, Z. Lu, C. He, J. Min, Structural basis for selective binding of m6A RNA by the YTHDC1 YTH domain. *Nat. Chem. Biol.* **10**, 927–929 (2014).
34. D. Martinez Molina, R. Jafari, M. Ignatushchenko, T. Seki, E. A. Larsson, C. Dan, L. Sreekumar, Y. Cao, P. Nordlund, Monitoring drug target engagement in cells and tissues using the cellular thermal shift assay. *Science* **341**, 84–87 (2013).
35. J. H. Lee, R. Wang, F. Xiong, J. Krakowiak, Z. Liao, P. T. Nguyen, E. V. Moroz-Omori, J. Shao, X. Zhu, M. J. Bolt, H. Wu, P. K. Singh, M. Bi, C. J. Shi, N. Jamal, G. Li, R. Mistry, S. Y. Jung, K. L. Tsai, J. C. Ferreon, F. Stossi, A. Caflisch, Z. Liu, M. A. Mancini, W. Li, Enhancer RNA m6A methylation facilitates transcriptional condensate formation and gene activation. *Mol. Cell* **81**, 3368–3385.e9 (2021).
36. K. Cermakova, H. C. Hodges, Next-generation drugs and probes for chromatin biology: From targeted protein degradation to phase separation. *Molecules* **23**, 10.3390/molecules23081958 (2018).

37. S. Yun, N. D. Vincelette, X. Yu, G. W. Watson, M. R. Fernandez, C. Yang, T. Hitosugi, C. H. Cheng, A. R. Freischel, L. Zhang, W. Li, H. Hou, F. X. Schaub, A. R. Vedder, L. Cen, K. L. McGraw, J. Moon, D. J. Murphy, A. Ballabio, S. H. Kaufmann, A. E. Berglund, J. L. Cleveland, TFEB links MYC signaling to epigenetic control of myeloid differentiation and acute myeloid leukemia. *Blood Cancer Discov.* **2**, 162–185 (2021).
38. S. Pei, M. Minhajuddin, B. Adane, N. Khan, B. M. Stevens, S. C. Mack, S. Lai, J. N. Rich, A. Inguva, K. M. Shannon, H. Kim, A. C. Tan, J. R. Myers, J. M. Ashton, T. Neff, D. A. Pollyea, C. A. Smith, C. T. Jordan, AMPK/FIS1-mediated mitophagy is required for self-renewal of human AML stem cells. *Cell Stem Cell* **23**, 86–100.e6 (2018).
39. D. A. Pollyea, C. T. Jordan, Therapeutic targeting of acute myeloid leukemia stem cells. *Blood* **129**, 1627–1635 (2017).
40. C. D. DiNardo, B. A. Jonas, V. Pullarkat, M. J. Thirman, J. S. Garcia, A. H. Wei, M. Konopleva, H. Döhner, A. Letai, P. Fenaux, E. Koller, V. Havelange, B. Leber, J. Esteve, J. Wang, V. Pejsa, R. Hájek, K. Porkka, Á. Illés, D. Lavie, R. M. Lemoli, K. Yamamoto, S. S. Yoon, J. H. Jang, S. P. Yeh, M. Turgut, W. J. Hong, Y. Zhou, J. Potluri, K. W. Pratz, Azacitidine and venetoclax in previously untreated acute myeloid leukemia. *N. Engl. J. Med.* **383**, 617–629 (2020).
41. S. Pei, D. A. Pollyea, A. Gustafson, B. M. Stevens, M. Minhajuddin, R. Fu, K. A. Riemondy, A. E. Gillen, R. M. Sheridan, J. Kim, J. C. Costello, M. L. Amaya, A. Inguva, A. Winters, H. Ye, A. Krug, C. L. Jones, B. Adane, N. Khan, J. Ponder, J. Schowinsky, D. Abbott, A. Hammes, J. R. Myers, J. M. Ashton, T. Nemkov, A. D'Alessandro, J. A. Gutman, H. E. Ramsey, M. R. Savona, C. A. Smith, C. T. Jordan, Monocytic subclones confer resistance to venetoclax-based therapy in patients with acute myeloid leukemia. *Cancer Discov.* **10**, 536–551 (2020).
42. D. Sharon, S. Cathelin, S. Mirali, J. M. Di Trani, D. J. Yanofsky, K. A. Keon, J. L. Rubinstein, A. D. Schimmer, T. Ketela, S. M. Chan, Inhibition of mitochondrial translation overcomes venetoclax resistance in AML through activation of the integrated stress response. *Sci. Transl. Med.* **11**, eaax2863 (2019).
43. C. Bosc, E. Saland, A. Bousard, N. Gadaud, M. Sabatier, G. Cognet, T. Farge, E. Boet, M. Gotanègre, N. Aroua, P. L. Mouchel, N. Polley, C. Larrue, E. Kaphan, M. Picard, A. Sahal, L. Jarrou, M. Tosolini, F. Rambow, F. Cabon, N. Nicot, L. Poillet-Perez, Y. Wang, X. Su, Q. Fovez, J. Kluza, R. J. Argüello, C. Mazzotti, H. Avet-Loiseau, F. Vergez, J. Tamburini, J. J. Fournié, I. S. Tiong, A. H. Wei, T. Kaoma, J. C. Marine, C. Récher, L. Stuani, C. Joffre, J. E. Sarry, Mitochondrial inhibitors circumvent adaptive resistance to venetoclax and cytarabine combination therapy in acute myeloid leukemia. *Nat. Cancer* **2**, 1204–1223 (2021).
44. X. Xiong, C. Yi, J. Peng, Epitranscriptomics: Toward a better understanding of RNA modifications. *Genomics Proteomics Bioinformatics* **15**, 147–153 (2017).
45. P. Nombela, B. Miguel-López, S. Blanco, The role of m^6A, m^5C and Ψ RNA modifications in cancer: Novel therapeutic opportunities. *Mol. Cancer* **20**, 18 (2021).
46. P. Boccaletto, F. Stefaniak, A. Ray, A. Cappannini, S. Mukherjee, E. Purta, M. Kurkowska, N. Shirvanizadeh, E. Destefanis, P. Groza, G. Avşar, A. Romitelli, P. Pir, E. Dassi, S. G. Conticello, F. Aguilo, J. M. Bujnicki, MODOMICS: A database of RNA modification pathways. 2021 update. *Nucleic Acids Res.* **50**, D231–D235 (2022).
47. J. Tong, G. Cao, T. Zhang, E. Sefik, M. C. Amezcua Vesely, J. P. Broughton, S. Zhu, H. Li, B. Li, L. Chen, H. Y. Chang, B. Su, R. A. Flavell, H. B. Li, m^6A mRNA methylation sustains Treg suppressive functions. *Cell Res.* **28**, 253–256 (2018).
48. L. P. Vu, B. F. Pickering, Y. Cheng, S. Zaccara, D. Nguyen, G. Minuesa, T. Chou, A. Chow, Y. Saletore, M. MacKay, J. Schulman, C. Famulare, M. Patel, V. M. Klimek, F. E. Garrett-Bakelman, A. Melnick, M. Carroll, C. E. Mason, S. R. Jaffrey, M. G. Kharas, The N^6-methyladenosine (m^6A)-forming enzyme METTL3 controls myeloid differentiation of normal hematopoietic and leukemia cells. *Nat. Med.* **23**, 1369–1376 (2017).
49. Y. Liu, G. Liang, H. Xu, W. Dong, Z. Dong, Z. Qiu, Z. Zhang, F. Li, Y. Huang, Y. Li, J. Wu, S. Yin, Y. Zhang, P. Guo, J. Liu, J. J. Xi, P. Jiang, D. Han, C. G. Yang, M. M. Xu, Tumors exploit FTO-mediated regulation of glycolytic metabolism to evade immune surveillance. *Cell Metab.* **33**, 1221–1233.e11 (2021).
50. C. Shen, Y. Sheng, A. C. Zhu, S. Robinson, X. Jiang, L. Dong, H. Chen, R. Su, Z. Yin, W. Li, X. Deng, Y. Chen, Y. C. Hu, H. Weng, H. Huang, E. Prince, C. R. Cogle, M. Sun, B. Zhang, C. W. Chen, G. Marcucci, C. He, Z. Qian, J. Chen, RNA demethylase ALKBH5 selectively promotes tumorigenesis and cancer stem cell self-renewal in acute myeloid leukemia. *Cell Stem Cell* **27**, 64–80.e9 (2020).
51. Z. Liu, T. Wang, Y. She, K. Wu, S. Gu, L. Li, C. Dong, C. Chen, Y. Zhou, N^6-methyladenosine-modified circIGF2BP3 inhibits $CD8^+$ T-cell responses to facilitate tumor immune evasion by promoting the deubiquitination of PD-L1 in non-small cell lung cancer. *Mol. Cancer* **20**, 105 (2021).
52. J. Zhou, C. Bi, Y. Q. Ching, J. Y. Chooi, X. Lu, J. Y. Quah, S. H. Toh, Z. L. Chan, T. Z. Tan, P. S. Chong, W. J. Chng, Inhibition of LIN28B impairs leukemia cell growth and metabolism in acute myeloid leukemia. *J. Hematol. Oncol.* **10**, 138 (2017).
53. Y. Cheng, Z. Gao, T. Zhang, Y. Wang, X. Xie, G. Han, Y. Li, R. Yin, Y. Chen, P. Wang, J. Hu, T. Zhang, C. Guo, J. Chai, J. Wang, M. Cui, K. Gao, W. Liu, S. Yao, P. Lu, Z. Cao, Y. Zheng, J. Chang, Z. Liu, Q. Song, W. Li, F. Zhou, H. Zhang, Decoding m^6A RNA methylome identifies PRMT6-regulated lipid transport promoting AML stem cell maintenance. *Cell Stem Cell* **30**, 69–85.e7 (2023).
54. X. Wang, S. Cooper, H. E. Broxmeyer, R. Kapur, Transient regulation of RNA methylation in human hematopoietic stem cells promotes their homing and engraftment. *Leukemia* **37**, 453–464 (2023).
55. C. Mapperley, L. N. van de Lagemaat, H. Lawson, A. Tavosanis, J. Paris, J. Campos, D. Wotherspoon, J. Durko, A. Sarapuu, J. Choe, I. Ivanova, D. S. Krause, A. von Kriegsheim, C. Much, M. Morgan, R. I. Gregory, A. J. Mead, D. O'Carroll, K. R. Kranc, The mRNA m^6A reader YTHDF2 suppresses proinflammatory pathways and sustains hematopoietic stem cell function. *J. Exp. Med.* **218**, e20200829 (2021).
56. S. Zaccara, S. R. Jaffrey, A unified model for the function of YTHDF proteins in regulating m^6A-modified mRNA. *Cell* **181**, 1582–1595.e18 (2020).
57. Y. Xu, W. Zhang, F. Shen, X. Yang, H. Liu, S. Dai, X. Sun, J. Huang, Q. Guo, YTH domain proteins: A family of m^6A readers in cancer progression. *Front. Oncol.* **11**, 629560 (2021).
58. X. Deng, Y. Qing, D. Horne, H. Huang, J. Chen, The roles and implications of RNA m^6A modification in cancer. *Nat. Rev. Clin. Oncol.* **20**, 507–526 (2023).
59. M. Sun, X. Zhang, Epigenetic regulation of N6-methyladenosine modifications in obesity. *J. Diabetes Investig.* **12**, 1306–1315 (2021).
60. Y. Qin, B. Li, S. Arumugam, Q. Lu, S. M. Mankash, J. Li, B. Sun, J. Li, R. A. Flavell, H. B. Li, X. Ouyang, m^6A mRNA methylation-directed myeloid cell activation controls progression of NAFLD and obesity. *Cell Rep.* **37**, 109968 (2021).
61. K. Ding, Z. Zhang, Z. Han, L. Shi, X. Li, Y. Liu, Z. Li, C. Zhao, Y. Cui, L. Zhou, B. Xu, W. Zhou, Y. Zhao, Z. Wang, H. Huang, L. Xie, X. W. Chen, Z. Chen, Liver ALKBH5 regulates glucose and lipid homeostasis independently through GCGR and mTORC1 signaling. *Science* **387**, eadp4120 (2025).
62. L. Jiang, W. Lin, C. Zhang, P. E. A. Ash, M. Verma, J. Kwan, E. van Vliet, Z. Yang, A. L. Cruz, S. Boudeau, B. F. Maziuk, S. Lei, J. Song, V. E. Alvarez, S. Hovde, J. F. Abisambra, M. H. Kuo, N. Kanaan, M. E. Murray, J. F. Crary, J. Zhao, J. X. Cheng, L. Petrucelli, H. Li, A. Emili, B. Wolozin, Interaction of tau with HNRNPA2B1 and N^6-methyladenosine RNA mediates the progression of tauopathy. *Mol. Cell* **81**, 4209–4227.e12 (2021).
63. R. Su, L. Dong, Y. Li, M. Gao, L. Han, M. Wunderlich, X. Deng, H. Li, Y. Huang, L. Gao, C. Li, Z. Zhao, S. Robinson, B. Tan, Y. Qing, X. Qin, E. Prince, J. Xie, H. Qin, W. Li, C. Shen, J. Sun, P. Kulkarni, H. Weng, H. Huang, Z. Chen, B. Zhang, X. Wu, M. J. Olsen, M. Müschen, G. Marcucci, R. Salgia, L. Li, A. T. Fathi, Z. Li, J. C. Mulloy, M. Wei, D. Horne, J. Chen, Targeting FTO Suppresses Cancer Stem Cell Maintenance and Immune Evasion. *Cancer Cell* **38**, 79–96.e11 (2020).
64. Y. Huang, R. Su, Y. Sheng, L. Dong, Z. Dong, H. Xu, T. Ni, Z. S. Zhang, T. Zhang, C. Li, L. Han, Z. Zhu, F. Lian, J. Wei, Q. Deng, Y. Wang, M. Wunderlich, Z. Gao, G. Pan, D. Zhong, H. Zhou, N. Zhang, J. Gan, H. Jiang, J. C. Mulloy, Z. Qian, J. Chen, C.-G. Yang, Small-molecule targeting of oncogenic FTO demethylase in acute myeloid leukemia. *Cancer Cell* **35**, 677–691.e10 (2019).
65. E. Yankova, W. Blackaby, M. Albertella, J. Rak, E. De Braekeleer, G. Tsagkogeorga, E. S. Pilka, D. Aspris, D. Leggate, A. G. Hendrick, N. A. Webster, B. Andrews, R. Fosbeary, P. Guest, N. Irigoyen, M. Eleftheriou, M. Gozdecka, J. M. L. Dias, A. J. Bannister, B. Vick, I. Jeremias, G. S. Vassiliou, O. Rausch, K. Tzelepis, T. Kouzarides, Small-molecule inhibition of METTL3 as a strategy against myeloid leukaemia. *Nature* **593**, 597–601 (2021).
66. S. Peng, W. Xiao, D. Ju, B. Sun, N. Hou, Q. Liu, Y. Wang, H. Zhao, C. Gao, S. Zhang, R. Cao, P. Li, H. Huang, Y. Ma, Y. Wang, W. Lai, Z. Ma, W. Zhang, S. Huang, H. Wang, Z. Zhang, L. Zhao, T. Cai, Y. L. Zhao, F. Wang, Y. Nie, G. Zhi, Y. G. Yang, E. E. Zhang, N. Huang, Identification of entacapone as a chemical inhibitor of FTO mediating metabolic regulation through FOXO1. *Sci. Transl. Med.* **11**, eaau7116 (2019).
67. L. Wang, X. Dou, S. Chen, X. Yu, X. Huang, L. Zhang, Y. Chen, J. Wang, K. Yang, J. Bugno, S. Pitroda, X. Ding, A. Piffko, W. Si, C. Chen, H. Jiang, B. Zhou, S. J. Chmura, C. Luo, H. L. Liang, C. He, R. R. Weichselbaum, YTHDF2 inhibition potentiates radiotherapy antitumor efficacy. *Cancer Cell* **41**, 1294–1308.e8 (2023).
68. Z. Chen, C. Zeng, L. Yang, Y. Che, M. Chen, L. Sau, B. Wang, K. Zhou, Y. Chen, Y. Qing, C. Shen, T. Zhang, M. Wunderlich, D. Wu, W. Li, K. Wang, K. Leung, M. Sun, T. Tang, X. He, L. Zhang, S. Swaminathan, J. C. Mulloy, M. Müschen, H. Huang, H. Weng, G. Xiao, X. Deng, J. Chen, YTHDF2 promotes ATP synthesis and immune evasion in B cell malignancies. *Cell* **188**, 331–351.e30 (2025).
69. A. Dolbois, R. K. Bedi, E. Bochenkova, A. Müller, E. V. Moroz-Omori, D. Huang, A. Caflisch, 1,4,9-Triazaspiro[5.5]undecan-2-one derivatives as potent and selective METTL3 inhibitors. *J. Med. Chem.* **64**, 12738–12760 (2021).
70. D. Dominissini, S. Moshitch-Moshkovitz, M. Salmon-Divon, N. Amariglio, G. Rechavi, Transcriptome-wide mapping of N^6-methyladenosine by m^6A-seq based on immunocapturing and massively parallel sequencing. *Nat. Protoc.* **8**, 176–189 (2013).
71. D. Kim, J. M. Paggi, C. Park, C. Bennett, S. L. Salzberg, Graph-based genome alignment and genotyping with HISAT2 and HISAT-genotype. *Nat. Biotechnol.* **37**, 907–915 (2019).
72. J. Meng, Z. Lu, H. Liu, L. Zhang, S. Zhang, Y. Chen, M. K. Rao, Y. Huang, A protocol for RNA methylation differential analysis with MeRIP-Seq data and exomePeak R/Bioconductor package. *Methods* **69**, 274–281 (2014).
73. S. Heinz, C. Benner, N. Spann, E. Bertolino, Y. C. Lin, P. Laslo, J. X. Cheng, C. Murre, H. Singh, C. K. Glass, Simple combinations of lineage-determining transcription factors prime

cis-regulatory elements required for macrophage and B cell identities. *Mol. Cell* **38**, 576–589 (2010).
74. M. Pertea, D. Kim, G. M. Pertea, J. T. Leek, S. L. Salzberg, Transcript-level expression analysis of RNA-seq experiments with HISAT, StringTie and Ballgown. *Nat. Protoc.* **11**, 1650–1667 (2016).
75. S. Kovaka, A. V. Zimin, G. M. Pertea, R. Razaghi, S. L. Salzberg, M. Pertea, Transcriptome assembly from long-read RNA-seq alignments with StringTie2. *Genome Biol.* **20**, 278 (2019).
76. M. Pertea, G. M. Pertea, C. M. Antonescu, T. C. Chang, J. T. Mendell, S. L. Salzberg, StringTie enables improved reconstruction of a transcriptome from RNA-seq reads. *Nat. Biotechnol.* **33**, 290–295 (2015).

Acknowledgments: We thank S. Huang (Department of Biochemistry and Molecular Biology, Louisiana State University Health Sciences Center, Shreveport, LA, USA) for careful proofreading. We also thank the staff from beamlines BL18U1 and BL19U1 at Shanghai Synchrotron Radiation Facility (SSRF) of the National Facility for Protein Science (Shanghai, China) for great support. **Funding:** This work was supported by the National Key R&D Program of China (2023YFF1204905); the National Natural Science Foundation of China (82273787 to L. Li, T2221004 to S.Y., 82373716 and 22207080 to Yueshan Li, and 82270157 and 82470149 to S.P.); the New Cornerstone Science Foundation; 1.3.5 Project for Disciplines of Excellence, West China Hospital, Sichuan University (ZYGD23006); grants from the Department of Science and Technology of Zhejiang Province (2023R01012) and the Basic Public Welfare Research Plan of Zhejiang (Q24H080022); the Natural Science Foundation of Xiamen (3502Z202472032); and the Natural Science Foundation of Fujian Province (2025J01330584). **Author contributions:** S.Y. initiated the project. S.Y., S.P., and L. Li conceived and supervised the research. S.Y., S.P., L. Li, H. Zhang, Yueshan Li, F.W., Y.Z., L. Liu, and G.L. designed the experiments. S.Y. and Yueshan Li performed the drug design. Yueshan Li, F.W., R. Yang, M.C., H.X., and J.Y. carried out the chemical synthesis and collected the data. H. Zhang, Yueyue Li, and R. Yao performed gene expression and protein purification, crystallization, and diffraction data collection. H. Zhang determined and analyzed the crystal structures. H. Zhang performed in vitro bioactivity assays, high-throughput drug screening, and IC_{50} measurements. H. Zhang, Y.Z., G.L., Yueyue Li, P.Z., M.W., C.T., S.L., and Y. Liao performed in vivo anti-AML assays, PK, and safety evaluations. H. Zhou, Y. Liang, L. Liu, and Y.S. performed the bioinformatics analysis. T.N., H.L., Y. Liao, Y. Yi, Y. Ye, C.Y., Y.H., and A.Z. provided the patient samples. S.Y., S.P., C.C., and L. Li analyzed and discussed the data. S.Y., S.P., H. Zhang, Yueshan Li, Y.Z., L. Liu, and G.L. wrote the manuscript. **Competing interests:** Sichuan University has applied for PCT patent application (PCT/CN2024/081963) and Chinese patent (202480003223.5) covering YL-5092 and related compounds. The other authors declare that they have no competing interests. **Data, code, and materials availability:** All data associated with this study are present in the paper or the Supplementary Materials. The atomic coordinates and structure factors (codes 9V84 and 9MB3) have been deposited in the Protein Data Bank (www.rcsb.org/). Data from RNA-seq, RIBO-seq, SLAM-seq, and m^6A-seq experiments have been deposited in the Genome Sequence Archive (https://ngdc.cncb.ac.cn/gsa-human/) under accession number HRA014685. The code used to analyze the sequencing data has been deposited in Zenodo (https://doi.org/10.5281/zenodo.18015358). Compound YL-5092 can be made available via a material transfer agreement upon request to the corresponding author. All other materials used or generated in this study are commercially available or will be supplied upon reasonable request.

Submitted 6 November 2024
Resubmitted 26 August 2025
Accepted 12 January 2026
Published 4 February 2026
10.1126/scitranslmed.adu3137

Science Translational Medicine

Small-molecule inhibition of YTHDC1 as a strategy against acute myeloid leukemia in mouse models

Hailin Zhang, Yueshan Li, Yin Zhao, Falu Wang, Guifeng Lin, Ting Niu, He Li, Yueyue Li, Lina Liu, Yue Liang, Yu Shen, Yuyao Yi, Hui Zhou, Shang Lou, Yishan Ye, Yanmin He, Ruicheng Yang, Rui Yao, Chenyu Tian, Pei Zhou, Mengdan Wu, Mingxin Chen, Haixing Xu, Jing You, Yi Liao, Chenlu Yang, Ailin Zhao, Chong Chen, Linli Li, Shanshan Pei, and Shengyong Yang

Sci. Transl. Med. **18** (835), eadu3137. DOI: 10.1126/scitranslmed.adu3137

Editor's summary

N6-methyladenosine (m6A) is a common posttranscriptional modification of mRNA and is recognized and bound by m6A reader proteins, which can then affect mRNA regulation and fate. Dysregulation of m6A readers is associated with the progression of various cancers, and here, Zhang *et al.* developed and characterized a selective first-in-class inhibitor of YTHDC1, a nuclear RNA m6A reader. In models of acute myeloid leukemia (AML), their compound, YL-5092, blocked the binding of YTHDC1 to m6A substrates and resulted in the apoptosis of AML cells. In mice, YL-5092 reduced the progression of leukemia and increased survival. This work demonstrates the therapeutic potential of targeting an m6A reader in the treatment of AML. —Amy E. Baek